Scientific report; WR-2000-03

KNMI

Salmon's Hamiltonian approach to balanced flow applied to a one-layer isentropic model of the atmosphere

W.T.M. Verkley

Koninklijk Nederlands Meteorologisch Instituut

De Bilt, 2000

Scientific report = Wetenschappelijk rapport; WR 2000-03

De Bilt, 2000

PO Box 201
3730 AE De Bilt
Wilhelminalaan 10
Telephone +31 30 220 69 11
Telefax +31 30 221 04 07

Author: Verkley, W.T.M.

UDC: 551.511.13
551.509.3

ISSN: 0169-1651

ISBN: 90-369-2177-5

Salmon's Hamiltonian approach to balanced flow applied to a one-layer isentropic model of the atmosphere

By W.T.M. Verkley*

Royal Netherlands Meteorological Institute, The Netherlands

July 2000

SUMMARY

Salmon's Hamiltonian approach is applied to formulate a balanced approximation to a hydrostatic one-layer isentropic model of the atmosphere. The model, referred to as the parent model, describes an idealized atmosphere of which the dynamics is closely analogous to a one-layer shallow-water model on the sphere. The balance used as input in Salmon's approach is a simplified form of 'linear balance', in which the balanced velocity $\mathbf{v}_b$ is given by $\mathbf{v}_b = \mathbf{k} \times \nabla f^{-1}(M - \bar{M})$. Here $\mathbf{k}$ is a vertical unit vector, f is the Coriolis parameter, M is the Montgomery potential and $\bar{M}$ is the value of the Montgomery potential at the state of rest. This form of balance behaves acceptably on the whole sphere, in contrast with 'classic' geostrophic balance, $\mathbf{v}_b = \mathbf{k} \times f^{-1}\nabla M$, which forces the meridional wind velocity to be zero at the equator. Salmon's Hamiltonian approach is applied to obtain an equation for the time-change of the balanced velocity that guarantees both material conservation of potential vorticity as well as conservation of energy. New in this application of Salmon's approach is a nonlinear relation between Montgomery potential and surface pressure (characteristic for an isentropic ideal gas in hydrostatic equilibrium) in combination with spherical geometry and a variable Coriolis parameter. We will discuss how the unbalanced velocity $\mathbf{v}_a$ can be calculated in a practical way and how the model can be stepped forward in time by advecting the balanced potential vorticity with the sum of the balanced and unbalanced velocity. The balanced model is tested against a ten-day period from a long integration with the parent model.

KEYWORDS: Isentropic atmosphere Hamilton's principle Balanced model

1. INTRODUCTION

In the present paper we apply Salmon's Hamiltonian approach (Salmon, 1983, 1985, 1988a, 1988b, 1996) to obtain a balanced approximation of a hydrostatic one-layer isentropic model of the atmosphere. The dynamics of an isentropic layer - a layer with uniform potential temperature - can be derived directly from the hydrostatic primitive equations on a rotating sphere (see Verkley, 2000). For the one-layer (parent) model discussed in the present paper, the governing equations are: an equation for the time-change of horizontal velocity (horizontal momentum per unit mass), an equation relating the Montgomery potential to the surface pressure, and an equation stating the conservation of mass. Due to the assumed constancy of potential temperature and the assumption of hydrostatic equilibrium, the absolute temperature in the model decreases linearly with height following the dry adiabatic lapse rate. The pressure and density decrease with height according to simple power laws whereas the Montgomery potential and the horizontal velocity are independent of height. The air in the model therefore moves column-wise between two material surfaces: a lower boundary with height z_l (given by the earth's orography) and an upper boundary with height z_u (determined by the condition of zero pressure). Due to the linear decrease of temperature with height, the value of z_u is finite. Apart from the nonlinear relation between Montgomery potential and surface pressure, the model equations are identical to the one-layer shallow-water equations on a rotating sphere with orography.

Our interest in this particular model, instead of the more familiar shallow-water model, is that discretisation of the atmosphere in terms of isentropic layers strains reality less than discretisation in terms of isopycnic layers. This is particulary true if one is

* Corresponding author: Royal Netherlands Meteorological Institute, P.O. Box 201, 3730 AE De Bilt, The Netherlands.

interested in models with a relatively small number of layers. Although very idealized, a single-layer atmosphere with constant potential temperature, evolving in time according to the equations mentioned above, is an exact solution of the inviscid hydrostatic primitive equations. Our confinement to a single layer is not necessary but is motived by practical considerations. We wish to concentrate on the new aspects that one encounters in applying Salmon's method to this type of model: a nonlinear relation between Montgomery potential and surface pressure, spherical geometry and a varying Coriolis parameter. Furthermore, instead of following Salmon by taking the 'classic' geostrophic relationship $\mathbf{v}_b = \mathbf{k} \times f^{-1} \nabla M$ as input in the method, we use for this purpose a simplification of 'linear balance': $\mathbf{v}_b = \mathbf{k} \times \nabla f^{-1}(M - \bar{M})$. The reason to do so is that 'classic' geostrophy is problematic on a sphere because it implies that the meridional wind velocity is zero at the equator. Our choice avoids this problem and, in addition, leads to a set of equations for the unbalanced velocity that is simpler than the corresponding set in the case of 'classic' geostrophy.

In section 2 we give the equations that govern the parent model, discuss its conservation laws and give Hamilton's principle for the model. In section 3 Salmon's method is applied to construct a balanced approximation. The central results are the momentum equation (22) and the set of equations (30)-(31) that determine the unbalanced velocity. It is checked that the balanced model has equivalents of the original conservation laws. In section 4 we discuss in more detail how the balanced model can be integrated forward in time. We have chosen to use the material conservation of balanced potential vorticity as our basic prognostic equation, and are thus confronted with an inversion problem that consists of two parts: solving for the balanced velocity from the balanced potential vorticity (which is a nonlinear problem) and solving for the unbalanced velocity from the balanced variables (which is a linear problem). In this respect our model is analogous to the 'slow equations' of Lynch (1989). In section 5 we discuss a long integration of the parent model, concentrating on a particular period of 10 days in which cyclogenesis occurs. It is checked whether the inversion procedure is able to reproduce from the potential vorticity field the flow field at the beginning of this period. We then integrate the balanced model forward in time for the same period of 10 days. The balanced model describes the time evolution in this period very accurately. By performing an integration in which the unbalanced velocity is put to zero, we demonstrate that inclusion of the latter is crucial for maintaining high accuracy. A summary and discussion can be found in section 6.

2. The parent model

The parent model is based on the hydrostatic primitive equations with no thermodynamic heating/cooling nor mechanical forcing/friction. These equations can be written in the form of three prognostic and three diagnostic equations. The prognostic equations are the conservation of thermodynamic energy, the conservation of mass and the time-change of horizontal momentum. The diagnostic equations are the definition of potential temperature, the ideal-gas law and the hydrostatic approximation. The basic assumption of the parent model is that the potential temperature θ is uniform throughout the atmosphere. Here $\theta = T(p_r/p)^\kappa$, where T is the absolute temperature, p is the pressure, p_r is a reference pressure of 1000 hPa and $\kappa = R/c_p$, where R is the gas constant for dry air and c_p is the specific heat of dry air at constant pressure. By combining the definition of potential temperature with the ideal gas law ($\rho = p/(RT)$, where ρ is the density) and the hydrostatic approximation ($\partial p/\partial z = -\rho g$, where z is the height above mean sea level and g is the acceleration due to gravity), it can be checked easily that

the absolute temperature T decreases linearly with height according to the dry adiabatic lapse rate $-g/c_p$. The pressure and density in a layer with uniform potential temperature decrease according to simple power laws of the absolute temperature: $p/p_r = (T/\theta)^{1/\kappa}$ and $\rho/\rho_r = (T/\theta)^{1/\kappa - 1}$. Here ρ_r is the density of the air at the reference pressure p_r, i.e., $\rho_r = p_r/(R\theta)$. Because the absolute temperature decreases linearly with height, a natural upper boundary is the (finite) height z_u at which the temperature, pressure and density are all equal to zero. The lower boundary is naturally formed by the height z_l of the orography. A schematic cross-section of the model is given in Fig. 1.

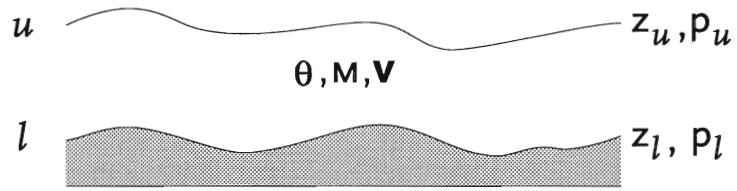

Figure 1. Schematic cross-section of the parent model. The model consists of a single layer of constant potential temperature and is governed by the hydrostatic primitive equations. The pressure p_u at the variable upper boundary z_u is assumed to have the fixed value zero. The pressure p_l at the lower boundary z_l is variable with the height z_l fixed by the orography. In a hydrostatic atmosphere in which the potential temperature θ is constant with height, the Montgomery potential M and the horizontal velocity $\mathbf{v}$ are also constant with height.

We will assume that the earth is perfectly spherical with radius a and that it rotates with angular velocity Ω. Horizontal positions on the sphere will be denoted by λ and ϕ, where λ is longitude and ϕ is latitude. The column-wise motion of the air is a consequence of the fact that the Coriolis parameter $f = 2\Omega \sin\phi$ and the Montgomery potential $M = gz + c_p T$ in the equation for the horizontal velocity $\mathbf{v}$ are independent of height. The horizontal velocity can therefore also be assumed independent of height. As a consequence the vertical advection of horizontal momentum is zero, so that the momentum equation reduces to

$$\frac{D\mathbf{v}}{Dt} + f\mathbf{k} \times \mathbf{v} + \nabla M = 0, \tag{1}$$

where D/Dt is the horizontal advection operator for a two-dimensional vector field on a spherical surface with radius a. If the Montgomery potential is evaluated at $z = z_l$ we have

$$M = gz_l + c_p \theta \eta_l^{\kappa}, \tag{2}$$

where we used the definition of potential temperature to express the absolute temperature at the lower boundary in terms of the pressure p. Variables at the upper and lower boundaries are denoted by the subscripts u and l, respectively, and for ease of notation and dimensional convenience we introduced the normalized pressure

$$\eta \equiv p/p_r. \tag{3}$$

An equation for the normalized surface pressure η_l follows from mass conservation:

$$\frac{D\eta_l}{Dt} + \eta_l(\nabla \cdot \mathbf{v}) = 0, \tag{4}$$

where D/Dt now denotes the horizontal material derivative for a scalar. The significance of this equation can be appreciated by realizing that the air moves column-wise, with material upper and lower boundaries, and that the the total mass per unit horizontal

area is given by $(p_r/g)\eta_l$ in a hydrostatic atmosphere with $\eta_u = 0$ as an upper boundary. The model (1), (2) and (4) forms a closed dynamical model in terms of $\mathbf{v}$, M and η_l. The model is closely analogous to a one-layer shallow water model, to which it actually reduces by taking $\kappa = 1$ and identifying $\eta_l(c_p\theta)/g$ with the fluid depth H. (Uniform potential temperature is then equivalent with uniform density.) In fact, in all equations that follow, we may obtain the shallow-water equivalents by substituting $\kappa = 1$. More details on the dynamics of an isentropic layer in hydrostatic equilibrium - of which the present model is a particular case - can be found in Verkley (2000).

(*a*) *Conservation laws of the parent model*

When we rewrite the mass conservation equation in flux form we have

$$\frac{\partial \eta_l}{\partial t} + \nabla \cdot [\eta_l \mathbf{v}] = 0. \tag{5}$$

It then follows immediately that the total mass m is conserved, where m is given by

$$m = \frac{p_r}{g} \int dS \eta_l. \tag{6}$$

Here $dS = a^2 \cos\phi d\lambda d\phi$ denotes an area element of the sphere. To investigate the conservation of potential vorticity and energy it is convenient to use the following formula for the material derivative of the horizontal velocity $\mathbf{v}$:

$$\frac{D\mathbf{v}}{Dt} = \frac{\partial \mathbf{v}}{\partial t} + \zeta(\mathbf{k} \times \mathbf{v}) + \nabla(\frac{\mathbf{v} \cdot \mathbf{v}}{2}). \tag{7}$$

The momentum equation can then be written as

$$\frac{\partial \mathbf{v}}{\partial t} + (f + \zeta)(\mathbf{k} \times \mathbf{v}) + \nabla(M + \frac{\mathbf{v} \cdot \mathbf{v}}{2}) = 0. \tag{8}$$

By applying the operators $\mathbf{k} \cdot \nabla\times$ and $\nabla\cdot$ to the equation above we obtain, respectively,

$$\frac{\partial \zeta}{\partial t} + \nabla \cdot [(f + \zeta)\mathbf{v}] = 0, \tag{9a}$$

$$\frac{\partial \mathcal{D}}{\partial t} + \nabla \cdot [(f + \zeta)(\mathbf{k} \times \mathbf{v}) + \nabla(M + \frac{\mathbf{v} \cdot \mathbf{v}}{2})] = 0, \tag{9b}$$

where $\zeta = \mathbf{k} \cdot \nabla \times \mathbf{v}$ is the vorticity and $\mathcal{D} = \nabla \cdot \mathbf{v}$ is the divergence of $\mathbf{v}$. From the vorticity equation (9a) one obtains an equation for the absolute vorticity $f + \zeta$

$$\frac{D}{Dt}(f + \zeta) + (f + \zeta)(\nabla \cdot \mathbf{v}) = 0, \tag{10}$$

and by eliminating the divergence from the mass conservation equation (4) and the absolute vorticity equation (10) we obtain

$$\frac{DP}{Dt} = 0, \quad P = \frac{f + \zeta}{\eta_l}. \tag{11}$$

This equation expresses the material conservation of the potential vorticity P. It can also be checked (see appendix A), using the momentum equation in the form (8) and the mass conservation equation in the form (5), that we have

$$\frac{\partial}{\partial t}[\eta_l(\frac{\mathbf{v} \cdot \mathbf{v}}{2} + g z_l + \frac{c_p\theta}{\kappa + 1}\eta_l^\kappa)] + \nabla \cdot [(M + \frac{\mathbf{v} \cdot \mathbf{v}}{2})\eta_l \mathbf{v}] = 0. \tag{12}$$

When this equation is integrated globally we obtain the conservation of total energy E, where E is given by

$$E = \frac{p_r}{g} \int dS \eta_l \left(\frac{\mathbf{v} \cdot \mathbf{v}}{2} + g z_l + \frac{c_p \theta}{\kappa + 1} \eta_l^{\kappa}\right). \tag{13}$$

These are the conservation laws of the parent model that we wish to retain in a balanced approximation.

(*b*) *Hamilton's principle for the parent model*

The basic idea of Salmon's approach to balanced flow (1983, 1985, 1988a, 1988b, 1996) is to cast the momentum equation in the form of Hamilton's principle and to make approximations in the Lagrangian. To formulate Hamilton's principle for the momentum equation of the parent model, Lagrangian column label fields α and β are introduced. These labels are, by definition, materially conserved. By equating the total mass per unit horizontal area to the Jacobian of these label fields, i.e., by taking

$$\left(\frac{p_r}{g}\right) \eta_l = \frac{1}{a^2 \cos\phi} \frac{\partial(\alpha, \beta)}{\partial(\lambda, \phi)}, \tag{14}$$

where

$$\frac{\partial(\alpha, \beta)}{\partial(\lambda, \phi)} = \frac{\partial \alpha}{\partial \lambda} \frac{\partial \beta}{\partial \phi} - \frac{\partial \alpha}{\partial \phi} \frac{\partial \beta}{\partial \lambda}, \tag{15}$$

we have that the mass conservation equation (5) is satisfied. Indeed, it can be checked explicitly that (5) follows from (14), (15) and $D\alpha/Dt = 0$ and $D\beta/Dt = 0$. Note that the expressions above imply that the total mass above an area element dS, which is given by $(p_r/g)\eta_l dS$, is given by $d\alpha d\beta$. Using the column label fields α and β Hamilton's principle for the parent model can be written as

$$\delta \int \int \int d\tau d\alpha d\beta \mathcal{L} = 0, \tag{16}$$

where

$$\mathcal{L} = (u + \Omega a \cos\phi) a \cos\phi \frac{\partial \lambda}{\partial \tau} + v a \frac{\partial \phi}{\partial \tau} - \mathcal{H}, \tag{17a}$$

and

$$\mathcal{H} = \frac{(u^2 + v^2)}{2} + g z_l + \frac{c_p \theta}{\kappa + 1} \eta_l^{\kappa}. \tag{17b}$$

Here u and v are the zonal and meridional components of the horizontal velocity $\mathbf{v}$. The variable τ is equal to the time t, but we note that it has a different role depending on whether we use (λ, ϕ, t) as Eulerian independent variables or (α, β, τ) as Lagrangian independent variables. A partial derivative in the first case is a local time derivative, whereas in the second case it is a material derivative. In the variational principle (16) the fields that are varied independently are u, v, λ and ϕ, considered as functions of α, β and τ. Variations of u and v lead to the definitions of the zonal and meridional components of the horizontal velocity in terms of the material derivatives of λ and ϕ. Variations of λ and ϕ give the zonal and meridional components of the momentum equation (1). More details can be found in appendix B.

3. The balanced model

A Hamiltonian balanced approximation of the momentum equation is obtained by substituting for u and v the zonal and meridional components u_b and v_b of a balanced velocity $\mathbf{v}_b$. Here 'balanced' is meant to denote any relation between wind field and mass field that eliminates gravity waves. As u_b and v_b are functions of λ and ϕ, the only variations to be considered are variations of λ and ϕ. For the balanced velocity we choose:

$$\mathbf{v}_b = \mathbf{k} \times \nabla \psi_b, \tag{18}$$

where $\mathbf{k}$ is a vertical unit vector and ψ_b is the streamfunction of the balanced flow. The balanced streamfunction is related to the Montgomery potential by

$$M = \bar{M} + f\psi_b, \tag{19}$$

where f is the Coriolis parameter and $\bar{M}$ is the value of the Montgomery potential at the state of rest. Expressions (18) and (19 are a simplification of 'linear balance' which Daley (1983) calls the simplest form of the geostrophic relationship. We note that (19) implies that the balanced streamfunction at the state of rest must be identicallly zero and that M must behave smoothly at the equator. Because the balanced velocity is nondivergent, there is no net balanced transport of air over any latitude circle, in particular over the equator. 'Classic' geostrophy, however, is more restrictive: it implies that the meridional wind velocity is zero at the equator. When (18) and (19) are combined we get $\mathbf{v}_b = \mathbf{k} \times \nabla f^{-1}(M - \bar{M})$. If f were constant this would be equivalent with $\mathbf{v}_b = \mathbf{k} \times f^{-1}\nabla M$, the expression for 'classic' geostrophic balance. However, when f does vary - in particular when it goes to zero at the equator - it makes much difference whether the factor f^{-1} is placed in front or after the gradient operator. Indeed, by calculating the divergence of the latter expression we readily verify that we have: $v_b = -a \tan\phi\ (\nabla \cdot \mathbf{v}_b)$. Because the divergence of any velocity field should be finite, this expression implies that $v_b = 0$ at $\phi = 0$. So, 'classic' geostrophic balance forces the equator to be a rigid impenetrable barrier between the hemispheres. As this is observationally unacceptable, 'classic' geostrophic balance - although a more obvious choice at first sight - does not suit our purpose.

(a) *Hamilton's principle for the balanced model*

An equation for the time-dependence of the balanced velocity follows from Hamilton's principle:

$$\delta \int\int\int d\tau d\alpha d\beta \mathcal{L}_b = 0, \tag{20}$$

where

$$\mathcal{L}_b = (u_b + \Omega a \cos\phi) a \cos\phi \frac{\partial \lambda}{\partial \tau} + v_b a \frac{\partial \phi}{\partial \tau} - \mathcal{H}_b, \tag{21a}$$

$$\mathcal{H}_b = \frac{(u_b^2 + v_b^2)}{2} + g z_l + \frac{c_p \theta}{\kappa + 1} \eta_l^{\kappa}. \tag{21b}$$

Calculating the variations with respect to λ and ϕ in (20) is a tedious task (for details we refer to appendix B). The result, however, is quite transparant and the variations with respect to λ and ϕ lead to the zonal and meridional components of the following momentum equation:

$$\frac{D_b \mathbf{v}_b}{Dt} + f\mathbf{k} \times \mathbf{v}_b + \nabla M +$$

$$(f + \zeta_b)\mathbf{k} \times \mathbf{v}_a + \nabla[(\xi_l f)^{-1}\mathbf{k} \cdot \nabla \times (\eta_l \mathbf{v}_a)] = 0. \tag{22}$$

Here D_b/Dt is the material derivative in which u and v are replaced by u_b and v_b. The velocity $\mathbf{v}_a$ is the unbalanced velocity defined by $\mathbf{v}_a = \mathbf{v} - \mathbf{v}_b$, where $\mathbf{v}$ is the true velocity in terms of material derivatives of λ and ϕ. We furthermore introduced, for ease of notation,

$$\xi \equiv \frac{\eta^{1-\kappa}}{\kappa c_p \theta}. \tag{23}$$

The subscript l means, as usual, that the field has to be evaluated at the lower boundary. When compared with the momentum equation (1) of the parent model we see that two additional terms have arisen: an extra Coriolis term and an extra gradient term, both of which are zero if the unbalanced velocity is zero. When the unbalanced velocity is nonzero, these terms are needed for potential vorticity and energy conservation.

(*b*) *The unbalanced velocity*

The unbalanced velocity can be obtained from the balanced fields by a diagnostic relation. This relation is obtained by first using (7) for the material derivative of the balanced velocity (with $\mathbf{v}$ replaced by $\mathbf{v}_b$) to rewrite the momentum equation as

$$\frac{\partial \mathbf{v}_b}{\partial t} + (f + \zeta_b)(\mathbf{k} \times \mathbf{v}) +$$

$$\nabla[M + \frac{\mathbf{v}_b \cdot \mathbf{v}_b}{2} + (\xi_l f)^{-1}\mathbf{k} \cdot \nabla \times (\eta_l \mathbf{v}_a)] = 0. \tag{24}$$

We then use the definition of the balanced velocity (18) and (19), in combination with expression (2) for M and the mass conservation equation (5) to obtain

$$\frac{\partial \mathbf{v}_b}{\partial t} = -\mathbf{k} \times \nabla[(\xi_l f)^{-1} \nabla \cdot (\eta_l \mathbf{v})]. \tag{25}$$

By eliminating $\partial \mathbf{v}_b/\partial t$ from both equations we find:

$$-\mathbf{k} \times \nabla[(\xi_l f)^{-1} \nabla \cdot (\eta_l \mathbf{v})] + (f + \zeta_b)(\mathbf{k} \times \mathbf{v}) +$$

$$\nabla[M + \frac{\mathbf{v}_b \cdot \mathbf{v}_b}{2} + (\xi_l f)^{-1}\mathbf{k} \cdot \nabla \times (\eta_l \mathbf{v}_a)] = 0, \tag{26}$$

which is the desired expression. To find a practical way to obtain the unbalanced velocity from this expression, we note that the first term on the left-hand side of (26) is divergenceless and that the third term is rotationless. By applying the Helmholtz decomposition to the middle term and using the vector identity $\mathbf{k} \cdot \nabla \times \mathbf{A} = -\nabla \cdot (\mathbf{k} \times \mathbf{A})$, we observe that (26) is equivalent with the following pair of scalar equations:

$$(\xi_l f)^{-1} \nabla \cdot (\eta_l \mathbf{v}) - \nabla^{-2} \nabla \cdot [(f + \zeta_b)\mathbf{v}] = 0, \tag{27a}$$

$$\nabla^{-2} \nabla \cdot [(f + \zeta_b)(\mathbf{k} \times \mathbf{v})] + f\psi_b + \frac{\mathbf{v}_b \cdot \mathbf{v}_b}{2} + (\xi_l f)^{-1}\mathbf{k} \cdot \nabla \times (\eta_l \mathbf{v}_a) = 0. \tag{27b}$$

To obtain these expressions we assumed that the result should also be valid at the state of rest, where $\mathbf{v} = 0$ and $M = \bar{M}$. We also used that $M = \bar{M} + f\psi_b$ and defined the inverse of the Laplacian to have a zero average. If we write $\mathbf{v} = \mathbf{v}_b + \mathbf{v}_a$, multiply by $\xi_l f$, use the balanced potential vorticity defined in (33) and carry out some rearranging, we can put these equations in the form:

$$\nabla \cdot (\eta_l \mathbf{v}_a) - \xi_l f \nabla^{-2} \nabla \cdot [P_b \eta_l \mathbf{v}_a] = S_\chi, \tag{28a}$$

$$\mathbf{k} \cdot \nabla \times (\eta_l \mathbf{v}_a) + \xi_l f \nabla^{-2} \nabla \cdot [P_b \mathbf{k} \times \eta_l \mathbf{v}_a] = S_\psi, \tag{28b}$$

where the terms S_χ and S_ψ are defined by

$$S_\chi = -\nabla \cdot (\eta_l \mathbf{v}_b) + \xi_l f \nabla^{-2} \nabla \cdot [(f + \zeta_b) \mathbf{v}_b], \tag{29a}$$

$$S_\psi = -\xi_l f (f \psi_b + \frac{\mathbf{v}_b \cdot \mathbf{v}_b}{2}) - \xi_l f \nabla^{-2} \nabla \cdot [(f + \zeta_b)(\mathbf{k} \times \mathbf{v}_b)]. \tag{29b}$$

If we finally use the Helmholtz decomposition of $\eta_l \mathbf{v}_a$,

$$\eta_l \mathbf{v}_a = \mathbf{k} \times \nabla \psi_a^{'} + \nabla \chi_a^{'}, \tag{30}$$

we can write

$$\nabla^2 \chi_a^{'} - \xi_l f \nabla^{-2} \nabla \cdot [P_b (\nabla \chi_a^{'} + \mathbf{k} \times \nabla \psi_a^{'})] = S_\chi, \tag{31a}$$

$$\nabla^2 \psi_a^{'} - \xi_l f \nabla^{-2} \nabla \cdot [P_b (\nabla \psi_a^{'} - \mathbf{k} \times \nabla \chi_a^{'})] = S_\psi. \tag{31b}$$

This is a linear system of equations that one can solve for $\chi_a^{'}$ and $\psi_a^{'}$. By dividing (30) by η_l and again applying an Helmholtz decomposition, we can obtain the fields ψ_a and χ_a of the Helmholtz decomposition of the unbalanced velocity itself.

(c) *Conservation laws of the balanced model*

Salmon's Hamiltonian approach guarantees that both energy and potential vorticity conservation have their counterparts in the balanced model. Mass remains to be conserved because the mass conservation equation (4) is part of the balanced model. The material conservation of balanced potential vorticity can be verified easily. From the momentum equation in the form (24) we can obtain an equation for the balanced absolute vorticity by operating with $\mathbf{k} \cdot \nabla \times$ on this equation:

$$\frac{D}{Dt}(f + \zeta_b) + (f + \zeta_b)(\nabla \cdot \mathbf{v}) = 0. \tag{32}$$

This equation can be combined, in the usual way, with the mass conservation equation (4) to give the material conservation of the balanced potential vorticity,

$$\frac{DP_b}{Dt} = 0, \quad P_b = \frac{f + \zeta_b}{\eta_l}. \tag{33}$$

Concerning energy conservation, it is shown in appendix A that we have the following counterpart of the local energy conservation law (12)

$$\frac{\partial}{\partial t}[\eta_l (\frac{\mathbf{v}_b \cdot \mathbf{v}_b}{2} + g z_l + \frac{c_p \theta}{\kappa + 1} \eta_l^\kappa] + \nabla \cdot [(M + \frac{\mathbf{v}_b \cdot \mathbf{v}_b}{2}) \eta_l \mathbf{v}] +$$

$$\nabla \cdot [(\xi_l f)^{-1} \mathbf{k} \cdot \nabla \times (\eta_l \mathbf{v}_a)\, \eta_l \mathbf{v} + (\xi_l f)^{-1} \nabla \cdot (\eta_l \mathbf{v})\, \mathbf{k} \times \eta_l \mathbf{v}_a] = 0. \tag{34}$$

Integrated over the whole sphere, this equation implies that

$$E_b = \frac{p_r}{g} \int dS \eta_l (\frac{\mathbf{v}_b \cdot \mathbf{v}_b}{2} + g z_l + \frac{c_p \theta}{\kappa + 1} \eta_l^\kappa) \tag{35}$$

is conserved. The quantity E_b will be called the balanced energy.

4. Time integration of the balanced model

In the balanced model we have three prognostic scalar equations: Eq. (4) for the normalized surface pressure, Eq. (32) for the balanced absolute vorticity and Eq. (33) for the balanced potential vorticity. In the balanced model (subject to a particular condition) each one of these equations implies the validity of the others. To show this, note that from expression (2) of the Montgomery potential and expressions (18) and (19) of the balance relationship, in addition to the fact that $\zeta_b = \nabla^2\psi_b$, we obtain

$$(\xi_l f)^{-1}\frac{\partial \eta_l}{\partial t} - \nabla^{-2}\frac{\partial}{\partial t}(f + \zeta_b) = 0. \tag{36}$$

This equation can be combined with (27a) to give:

$$(\xi_l f)^{-1}[\frac{\partial \eta_l}{\partial t} + \nabla \cdot (\eta_l \mathbf{v})] - \nabla^{-2}[\frac{\partial}{\partial t}(f + \zeta_b) + \nabla \cdot ((f + \zeta_b)\mathbf{v})] = 0. \tag{37}$$

From this equation we observe that in the balanced model the validity of the equation for the normalized surface pressure implies the validity of the equation for the balanced absolute vorticity and vice versa. As we have just seen, the two equations together imply the material conservation of balanced potential vorticty. On the other hand, from the material conservation of balanced potential vorticity it can be deduced that

$$P_b[\frac{\partial \eta_l}{\partial t} + \nabla \cdot (\eta_l \mathbf{v})] - [\frac{\partial}{\partial t}(f + \zeta_b) + \nabla \cdot ((f + \zeta_b)\mathbf{v})] = 0. \tag{38}$$

Combining (37) and (38) we can derive that

$$[1 - \xi_l f \nabla^{-2} P_b][\frac{\partial \eta_l}{\partial t} + \nabla \cdot (\eta_l \mathbf{v})] = 0, \tag{39a}$$

$$[1 - \xi_l f P_b \nabla^{-2}][\frac{\partial}{\partial t}(f + \zeta_b) + \nabla \cdot ((f + \zeta_b)\mathbf{v})] = 0. \tag{39b}$$

(Note that in the first of the resulting expressions the inverse Laplacian is assumed to be applied to the product of P_b and the expression that follows.) So, in the balanced model the material conservation of balanced potential vorticity implies the conservation of mass as well as balanced absolute vorticity under the condition that the operators between square brackets are invertible. This is interesting from the viewpoint of time stepping, because it allows one to use either the mass conservation equation, the balanced absolute vorticity equation or the balanced potential vorticity equation to step the model forward in time. Time stepping in terms of the normalized surface pressure confronts us with the difficulty of finding ψ_b from η_l because one has to divide by f. Although not impossible, it means that extra smoothness conditions on M have to be maintained. Time stepping in terms of the balanced absolute vorticity avoids this difficulty because the streamfunction can then be readily obtained by inverting the Laplacian and finding the normalized surface pressure only involves a multiplication with f. We will, however, choose the third possibility because advection as the basic time stepping process allows the use of Lagrangian or semi-Lagrangian integration procedures which offer the best perspectives for a fast performance of the model.

So we will step the model forward in time by advecting the balanced potential vorticity P_b with the full velocity $\mathbf{v} = \mathbf{v}_b + \mathbf{v}_a$. We will now describe in more detail how - if such a time-step is made - the new velocity $\mathbf{v}$ can be obtained from the new potential vorticity P_b. Rewriting the definition of the potential vorticity we have

$$\nabla^2\psi_b = P_b\eta_l - f. \tag{40}$$

For η_l we have, combining (2) and (19),

$$\eta_l = (\frac{\bar{M} + f\psi_b - gz_l}{c_p\theta})^{1/\kappa}. \tag{41}$$

so that

$$\nabla^2\psi_b = P_b(\frac{\bar{M} + f\psi_b - gz_l}{c_p\theta})^{1/\kappa} - f. \tag{42}$$

This is a nonlinear equation that relates ψ_b to P_b. The value $\bar{M}$ is the value of the Montgomery potential at the state of rest. From the definition of the Montgomery potential we see that the state of rest is characterized by the following normalized surface pressure distribution:

$$\bar{\eta}_l = (\frac{\bar{M} - gz_l}{c_p\theta})^{1/\kappa}. \tag{43}$$

Now, if we use that the total mass m of the atmosphere is a given constant the expression above fixes $\bar{M}$ in terms of m because we have

$$m = \frac{p_r}{g}\int dS\eta_l = \frac{p_r}{g}\int dS\bar{\eta}_l = \frac{p_r}{g}\int dS(\frac{\bar{M} - gz_l}{c_p\theta})^{1/\kappa}. \tag{44}$$

In the numerical simulation to be discussed we start from the state of rest, where $\bar{\eta}_l$ is given by (43) with $\bar{M} = c_p\theta$. It is ensured in the integration that the mass does not change in time, so that $\bar{M}$ is and remains equal to $c_p\theta$.

The conditions under which (42) is formally solvable have not been investigated in detail. Experience has shown that an iteration procedure always leads to a solution. Furthermore, the resulting solution is unique to the extent that different first guesses do not lead to substantially different solutions. The iteration procedure, as actually implemented, starts with $\psi_b = 0$ as a first guess on the right-hand side of (42). Then ψ_b on the left-hand side is obtained by inverting the Laplace operator; subsequently ψ_b is updated by adding a fraction r of the difference between this and the previous field to ψ_b, after which the result is substituted back in the right-hand side of (42). We then again invert the Laplacian, etc., and continue the procedure until the required accuracy is obtained. From the resulting streamfunction ψ_b the fields ζ_b, $\mathbf{v}_b$, η_l and M can be obtained straightforwardly.

Having obtained the balanced flow variables we may solve equations (31) to determine the unbalanced velocity $\mathbf{v}_a$. We note that without the second terms on the left-hand side the system (31) consists of two uncoupled Poisson equations that are readily solvable. It is not clear whether the system is formally solvable if these terms are present but also here experience has shown that an iterative procedure always leads to a solution that is apparently unique. As first guesses for ψ_a' and χ_a' we take the fields that result from solving (31) without the second terms on the left-hand side and with $S_\chi = -\nabla\cdot(\eta_l\mathbf{v}_b)$ and $S_\psi = 0$. So the first guesses of χ_a' and ψ_a' satisfy

$$\nabla^2\chi_a' + \nabla\cdot(\eta_l\mathbf{v}_b) = 0, \tag{45a}$$

$$\nabla^2\psi_a' = 0. \tag{45b}$$

In the iteration procedure, the second terms on the left-hand side of (31) are treated as source terms in which fields ψ_a' and χ_a' from the previous iteration are substituted. The new ψ_a' and χ_a' are obtained by inverting the corresponding Laplacians, as in (42), after

which the fields are updated by adding a fraction r of the difference between the new fields and the previous fields. The procedure is repeated as many times as is considered necessary to get the required accuracy.

5. Numerical integrations

To have a reference against which the balanced model can be tested, we performed a long numerical integration of a spectral implementation of the parent model. Within this period a shorter period was selected during which cyclogenesis took place. We will check to what extent the balanced model is able to predict this phenomenon from an earlier initial state.

We first give some details on the spectral method that is used. We recall that the parent model is originally given by the momentum equation (1), expression (2) for the Montgomery potential and the mass conservation equation (4). The velocity field $\mathbf{v}$ is Helmholtz decomposed in terms of a divergenceless and a rotationless part, $\mathbf{v} = \mathbf{k} \times \nabla\psi + \nabla\chi$, where the streamfunction ψ and the velocity potential χ are related to the vorticity ζ and the divergence $\mathcal{D}$ by $\nabla^2\psi = \zeta$ and $\nabla^2\chi = \mathcal{D}$. Instead of the momentum equation we use equations (9) for the relative vorticity and the divergence. We furthermore use the mass conservation equation in the form (5) and expression (2) for the Montgomery potential. The parent model is thus formulated in terms of the scalar fields ζ, $\mathcal{D}$, η_l and M. In the numerical integration we will make use of Ω^{-1} and a as the units of time and length, respectively.

The scalar fields will be represented by spherical harmonics $Y_{mn}(\lambda, \phi)$, where m and n are integers with $n \geq |m|$. The spherical harmonics are normalized such that they are orthonormal with respect to the usual inner product $<\psi, \chi>= 1/(4\pi) \int dS\psi^*\chi$ for functions ψ and χ on a sphere, where the asterisk denotes complex conjugation and the integral is over the whole sphere. We will use a triangular $T42$ truncation, i.e., we use all spherical harmonics up to $n = 42$. Spherical harmonics are eigenfunctions of the Laplace operator with eigenvalues $-n(n+1)$, so that $\nabla^2\psi$ and its inverse $\nabla^{-2}\psi$ can be represented easily and exactly in terms of a diagonal matrix. The other operators are approximated by applying the operator on a Gaussian grid (equidistant in λ, Gaussian quadrature points for $\sin\phi$) and projecting the result on Y_{mn} by a summation over this grid. These operators are $\mathbf{k} \cdot \nabla\psi \times \nabla\chi$, $\nabla\psi \cdot \nabla\chi$, $\psi\chi$, ψ/χ and ψ^μ, where μ is positive real number. All operators encountered (also in the context of the balanced model) can be - and are actually - reduced to one of the operators mentioned above. We use a Gaussian grid of 128×64 points, as a result of which the projection is exact for the operators $\mathbf{k} \cdot \nabla\psi \times \nabla\chi$, $\nabla\psi \cdot \nabla\chi$ and $\psi\chi$. For more details on the spectral method for a sphere we refer to Machenhauer (1979).

(a) *A numerical integration of the parent model*

Using a fourth-order Runge-Kutta time-stepping scheme with a time-step of 5 minutes we integrate the model in time for a total period of 500 days. To suppress the emergence of spurious small-scale structures at the truncation limit we add a hyperviscosity term to both equations (9). More specifically, the evolution equations for the relative vorticity and the divergence become

$$\frac{\partial\zeta}{\partial t} + \nabla \cdot [(f+\zeta)\mathbf{v}] + \frac{1}{\tau_h}\nabla^{12}\zeta = 0, \tag{46a}$$

$$\frac{\partial\mathcal{D}}{\partial t} + \nabla \cdot [(f+\zeta)(\mathbf{k} \times \mathbf{v}) + \nabla(M + \frac{\mathbf{v} \cdot \mathbf{v}}{2})] + \frac{1}{\tau_h}\nabla^{12}\mathcal{D} = 0, \tag{46b}$$

where τ_h is chosen such that the spectral coefficients of ζ and $\mathcal{D}$ with $n = 42$ are damped with an e-folding time of 3 hours. In order to spin up the model it is furthermore forced to a zonal surface pressure distribution η_l^f. The mass conservation equation (5) therefore becomes

$$\frac{\partial \eta_l}{\partial t} + \nabla \cdot [\eta_l \mathbf{v}] + \frac{1}{\tau_f}(\eta_l - \eta_l^f) = 0, \tag{47}$$

where the e-folding time τ_f is 15 days and the surface pressure distribution η_l^f is given by

$$\eta_l^f(\phi) = \alpha^f + \beta^f[\cos 2\phi(\sin^2 2\phi + 2) - \frac{13}{16}]. \tag{48}$$

Here α^f is the mean value of the pressure distribution and β^f the strength of its meridional variation. For the parameters α^f and β^f we have taken 0.97482 and 0.05, respectively. A graph of η_l^f as a function of ϕ is given in Fig. 2a.

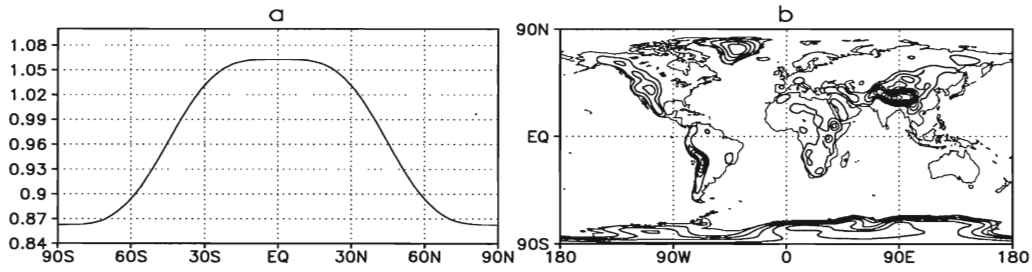

Figure 2. (a) Graph of η_l^f to which the normalized surface pressure distribution η_l of the parent model is forced in the numerical simulation. (b) The field gz_l in units of $a^2\Omega^2$ in the $T42$ trunctation of the spectral model. The contour interval is 0.03 with the zero contour deleted. The maximum values at Greenland, the Rocky Mountains, the Andes, Antarctica and the Himalayas are 0.12, 0.09, 0.15, 0.15 and 0.27, respectively.

The initial state of the integration is the state of rest with $\bar{\zeta} = 0$, $\bar{\mathcal{D}} = 0$ and $\bar{\eta}_l$ given by (43), with $\bar{M} = c_p\theta$. Note that with this choice the pressure field $\bar{\eta}_l$ at the state of rest has the value 1 at $z_l = 0$. The total mass of the atmosphere follows from (44). For the field z_l we use the $T42$ representation of the earth's orography. A plot of gz_l in units of $a^2\Omega^2$ is shown in Fig. 2b. With $c_p = 1005\text{JK}^{-1}\text{kg}^{-1}$, $R = 287.04\text{JK}^{-1}\text{kg}^{-1}$ (values taken from Dutton (1986, Appendix 3)) and $\theta = 300\text{K}$, we have $\kappa = R/c_p = 0.28561$ and $c_p\theta = 1.39694\, a^2\Omega^2$. The mean value of $\bar{\eta}_l$ is 0.97482; this is the value taken for α^f in expression (48). As a result, the forcing to the prescribed surface pressure, expressed by (47), does not change the total mass of the model atmosphere and therefore not the value of $\bar{M}$ which thus remains $c_p\theta$.

In the period from 83 to 93 days after the start of the integration a cyclogenesis process occurs as a result of interaction with the orography. We will concentrate on this period. To obtain a reference integration which is as close as possible to an inviscid integration we rerun the model for 10 days from day 83 with the forcing term in the mass conservation equation turned off. (The hyperviscosity term was retained in order to suppress small-scale structures.) The potential vorticity P and the velocity field $\mathbf{v}$ are shown in Fig. 3 at 6 times in this period of ten days: at 0, 2, 4, 6, 8 and 10 days after the rerun from day 83. The potential vorticity is calculated by evaluating the quotient of $f + \zeta$ and η_l on the Gaussian grid and projecting the result back to $T42$ by a summation over the grid - as with the other nonlinear operators. The differences between the original

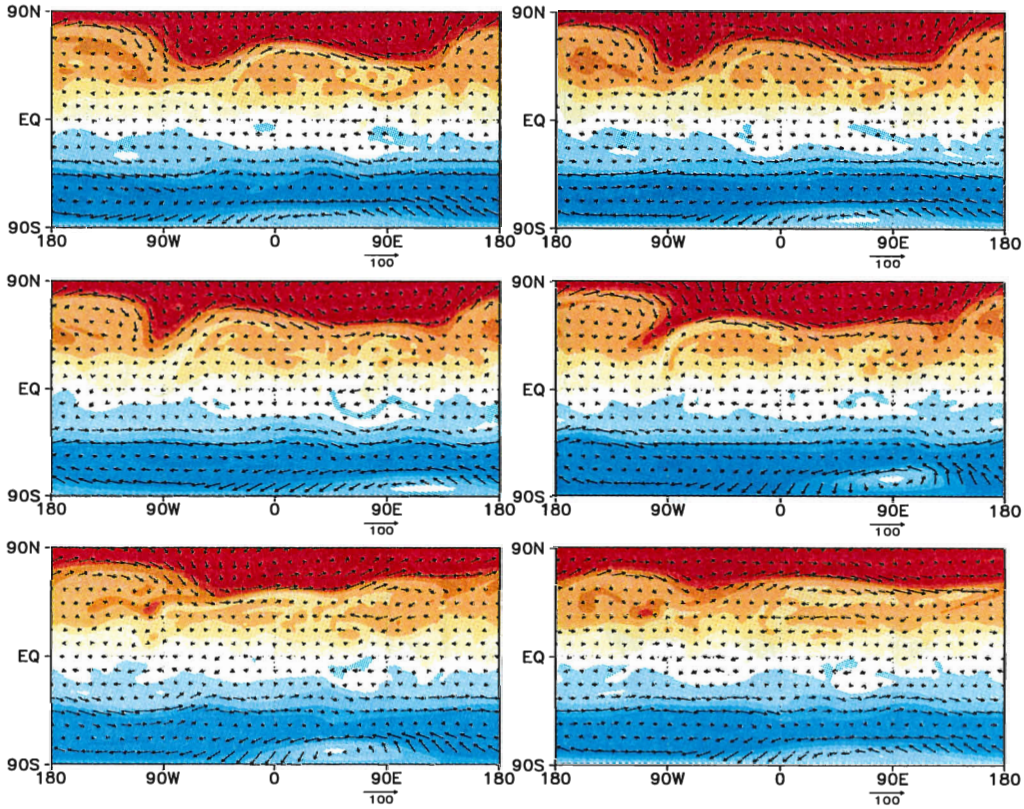

Figure 3. Results of the numerical integration of the parent model after 0, 2, 4, 6, 8 and 10 days - (a), (b), (c), (d), (e) and (f), respectively - from the start of the rerun, initialized with the fields after 83 days of the original integration. The rerun differs from the original integration in that the forcing to the prescribed zonal pressure distribution is turned off. The results are displayed in terms of potential vorticity (colours) and velocity (arrows). Here and in other plots of a similar type, the potential vorticity is plotted on a regular longitude-latitude grid of 128×64 points; the velocity vectors are displayed on the same type of grid but with 32×16 points. The contour interval in the plots of potential vorticity is 0.5; the values from -3.0 to -2.5 are coloured deep blue, the values from -2.5 to 2.0 somewhat lighter blue, etc., until the values from -0.5 to 0 that are coloured white; then the values from 0 to 0.5 are coloured light yellow, the values from 0.5 to 1.0 somewhat darker yellow, etc., until the values from 2.5 to 3.0 that are coloured deep red. This particular period was chosen because of the cyclogenesis process that occured within this period, leading to a cyclone at 90° West and 45° North around day 8.

simulation are not very large, except that in the original simulation the vortices that form in the process of wave breaking are dissipated somewhat faster. The cyclogenesis process manifests itself in the pinching off of potential vorticity around day 8. In Fig. 4 we show the other fields at day 0: (a) the relative vorticity ζ, (b) the streamfunction ψ, (c) the divergence $\mathcal{D}$, (d) the velocity potential χ, (e) the normalized surface pressure η_l and (f) the Montgomery potential M. We see that the divergence is an order of magnitude smaller than the relative vorticity. We also see that the relative vorticity has concentrated into well-defined bands (with corresponding jets), in particular at the Northern Hemisphere. The divergence is concentrated around the extrema in the orography.

(*b*) *A numerical integration of the balanced model*

The balanced model is governed by the advection of balanced potential vorticity,

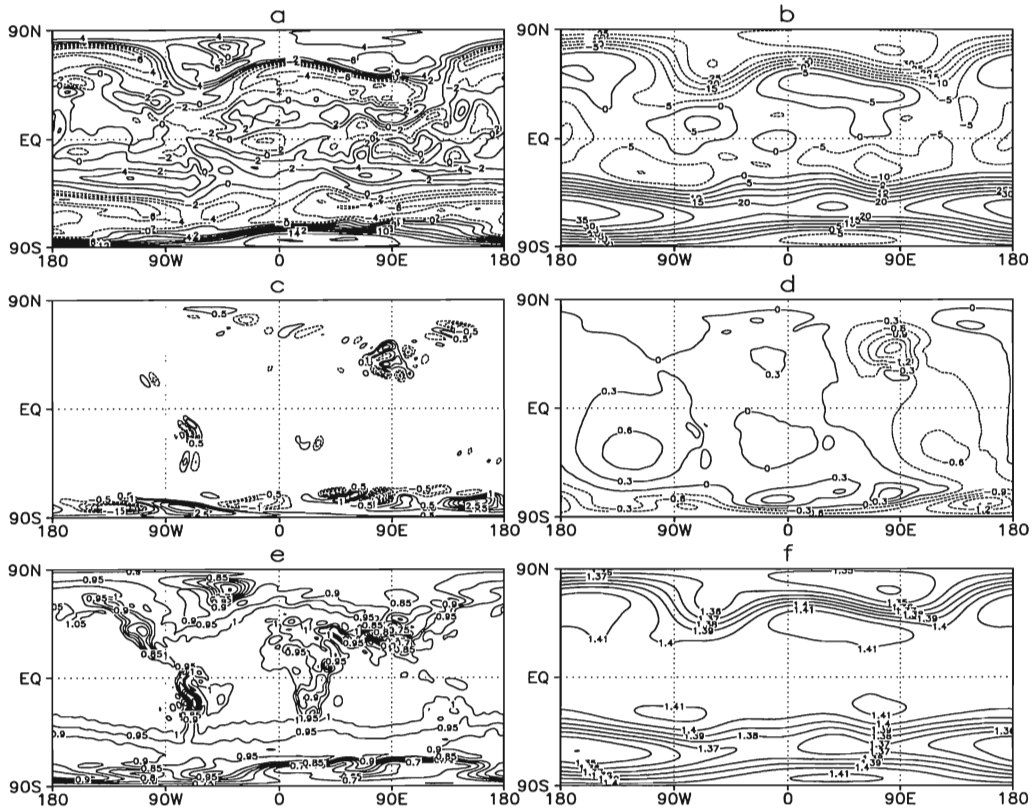

Figure 4. The other fields at day 0 of the model run of which the potential vorticity and velocity are shown in Fig. 3. In (a), (b), (c), etc. we show the relative vorticity ζ ($\times 10$), the streamfunction ψ ($\times 1000$), the divergence $\mathcal{D}$ ($\times 10$), the velocity potential χ ($\times 1000$), the normalized surface pressure η_l and the Montgomery potential M. The convention here and in other plots of a similar type is that solid isolines denote positive values and dashed isolines denote negative values. Note that the relative vorticity - in particular in the Northern Hemisphere - has concentrated into a well-defined band, and that the divergence is an order of magnitude smaller than the relative vorticity. The divergence is largest around high values of the orography.

as expressed by (33). We recall that this equation is based on the combination of the equations for the normalized surface pressure and the balanced absolute vorticity. When we add the forcing term to the equation for the normalized surface pressure and the hyperviscosity term to the equation for the balanced absolute vorticity (the ∇^{12} operator acting on the balanced relative vorticity), then we may again combine these equations into an equation for the balanced potential vorticity. This equation then becomes (writing out the material derivative)

$$\frac{\partial P_b}{\partial t} + \mathbf{v} \cdot \nabla P_b = \mathcal{S}, \tag{49}$$

where the source term $\mathcal{S}$ is given by

$$\eta_l \mathcal{S} = -\frac{1}{\tau_h} \nabla^2 \zeta_b + \frac{1}{\tau_f} P_b (\eta_l - \eta_l^f). \tag{50}$$

We have seen earlier that in the balanced model - without forcing or damping - the validity of the potential vorticity equation implies the validity of the normalized pressure

equation and the balanced absolute vorticity equation. This is now no longer the case in the sense that (49) does not imply the original equations for the normalized pressure and the vorticity, but instead (compare with (39))

$$[1 - \xi_l f \nabla^{-2} P_b][\frac{\partial \eta_l}{\partial t} + \nabla \cdot (\eta_l \mathbf{v})] = \xi_l f \nabla^{-2} \eta_l \mathcal{S}, \tag{51a}$$

$$[1 - \xi_l f P_b \nabla^{-2}][\frac{\partial}{\partial t}(f + \zeta_b) + \nabla \cdot ((f + \zeta_b)\mathbf{v})] = \eta_l \mathcal{S}. \tag{51b}$$

In the integration to be discussed we used (49) and (50) in which we have put the second term in the forcing $\mathcal{S}$ equal to zero.

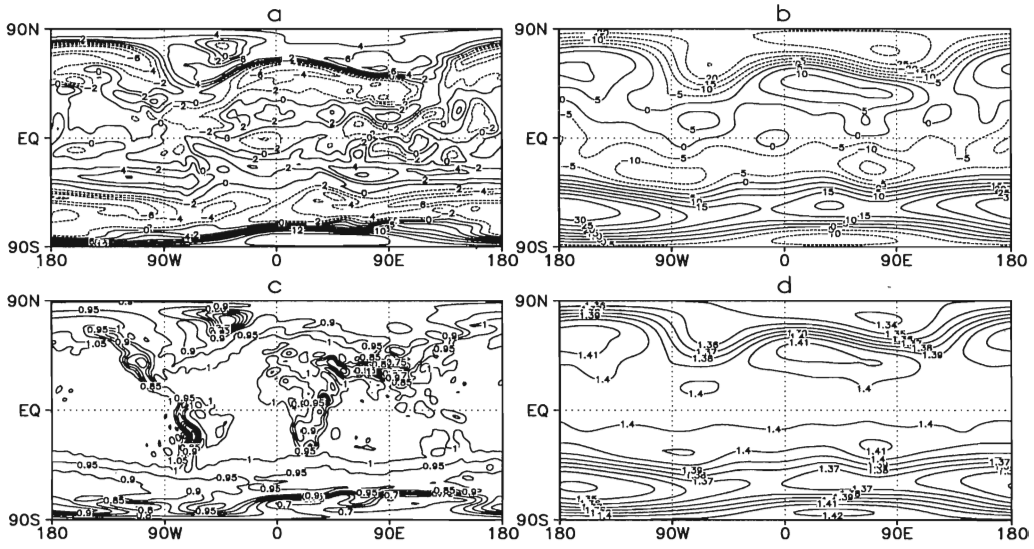

Figure 5. The balanced flow fields obtained from the potential vorticity as shown in Fig. 3a. In (a), (b), (c) and (d) we show the relative vorticity ζ_b ($\times 10$), the streamfunction ψ_b ($\times 1000$), the normalized surface pressure η_l and the Montgomery potential M.

Before discussing the result of the integration we will consider how well the balancing procedure is able to recover the fields as displayed in Fig. 4 from the potential vorticity field at day 0 (shown in Fig. 3a and identified with P_b). We begin by discussing the balanced fields. The balanced streamfunction ψ_b is calculated from (42) using the iteration procedure that is described in section 4. The iteration procedure is stopped if the norm (the square root of the inner product) of the update becomes smaller than 0.5 percent of the norm of the present field. With a relaxation factor $r = 0.3$ - an optimal value - the procedure finished after 14 iterations. The result is shown in Fig. 5, where (a), (b), (c) and (d) are ζ_b, ψ_b, η_l and M. We recall that M is calculated from ψ_b using (19) - with $\bar{M} = c_p \theta$ - whereas η_l is calculated from M using (2). When we compare Figs. 5a, 5b, 5c and 5d with Figs. 4a, 4b, 4e and 4f, respectively, we see that the fields obtained from P_b are close to their original counterparts.

By definition the balanced flow has zero divergence. The divergence field is obtained by solving (31) for the unbalanced part of the flow, using the method outlined in the previous section. We use a relaxation factor $r = 0.5$ and stop the iteration when the norms of both updates are smaller than 0.5 percent of the norms of the corresponding fields. The procedure needed 8 iterations to reach this criterium. From the fields ψ_a' and χ_a' we

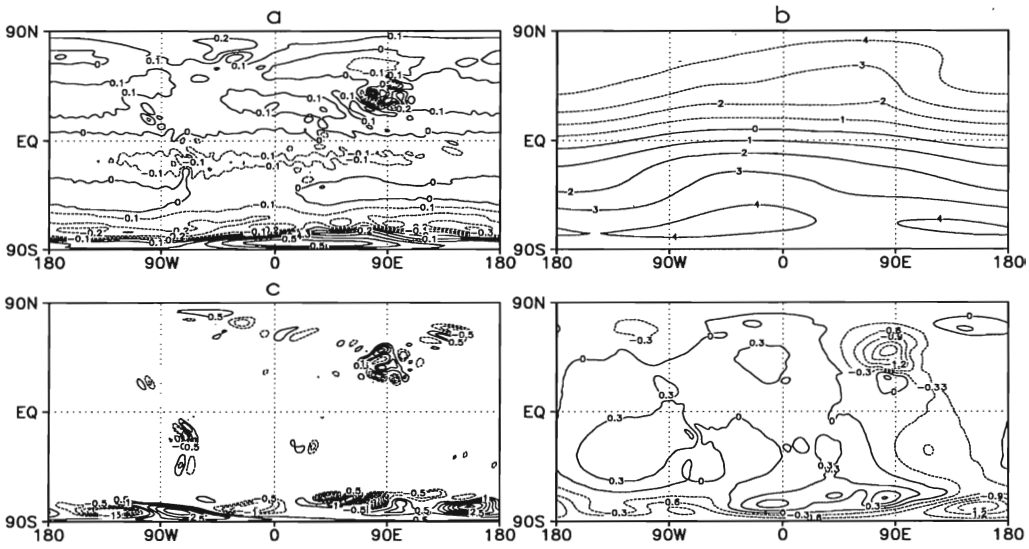

Figure 6. The unbalanced flow fields obtained from the potential vorticity as shown in Fig. 3a. In (a), (b), (c) and (d) we show the relative vorticity ζ_a ($\times 10$), the streamfunction ψ_a ($\times 1000$), the divergence $\mathcal{D}_a$ ($\times 10$) and the velocity potential χ_a ($\times 1000$).

obtain ψ_a and χ_a using the method outlined after (31). The divergence field is given by $\mathcal{D}_a = \nabla^2 \chi_a$. The result is shown in Fig. 6, where (a), (b), (c), and (d) are $\zeta_a = \nabla^2 \psi_a$, ψ_a, $\mathcal{D}_a = \nabla^2 \chi_a$ and χ_a. By comparing Fig. 6c and 6d with Fig. 4c and 4d we see that the divergence field is also recovered well.

To summarize: the panels (c) and (d) of Fig. 5 show the reconstruction of the fields η_l and M, respectively, and should be compared with the panels (e) and (f) of Fig. 4. The panels (c) and (d) of Fig. 6 show the reconstruction of the fields $\mathcal{D}$ and χ, respectively, and are to be compared with (c) and (d) of Fig. 4. The panels (a) and (b) of Fig. 6 show the unbalanced contributions to the fields ζ and ψ of which the balanced contributions are shown in the panels (a) and (b) of Fig. 5. For completeness we give the sum of the balanced and unbalanced contributions to ζ and ψ in the panels (a) and (b) of Fig. 7. The resemblance with the original fields, displayed in the panels (a) and (b) of Fig. 4, improves somewhat. However, a more detailed analysis shows that the relative vorticity field both slightly improves and deteriorates, depending on the position. The streamfunction, though, generally improves in the sense that the difference with the original field is reduced by more than 50 percent. Fig. 8 shows how well the velocity field $\mathbf{v}$ of the numerical integration is recovered by $\mathbf{v}_b$ and $\mathbf{v}_a$. In Fig. 8a we show $\mathbf{v} - \mathbf{v}_b$. We see that the balanced velocity field gives a reasonable approximation to $\mathbf{v}$, apart from the equatorial region and the regions with high values of the orography. It is here that the unbalanced velocity field helps to improve the resemblance, as can be seen from Fig. 8b, where we show $\mathbf{v} - \mathbf{v}_b - \mathbf{v}_a$.

From the potential vorticity P at day 0, identified with the balanced potential vorticity P_b, we have integrated our balanced model forward in time for 10 days. The results are very close to the results displayed in Fig. 3. Instead of showing the results in the format of Fig. 3, we show the result at day 10 and the difference with the parent integration at day 10 in Figs. 9a and 9b, respectively. The maximum absolute value of the difference between the potential vorticity of the balanced model and the potential vorticity of the

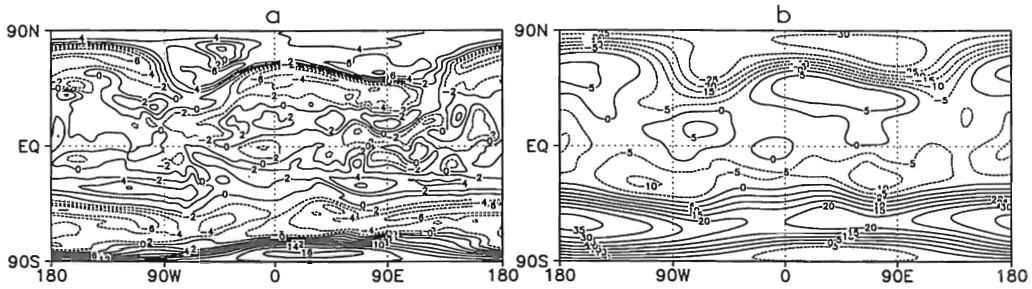

Figure 7. The sum of the balanced and unbalanced contribution to (a) the relative vorticity and (b) the streamfunction, i.e. in (a) the field $\zeta_b + \zeta_a$ is displayed and in (b) the field $\psi_b + \psi_a$.

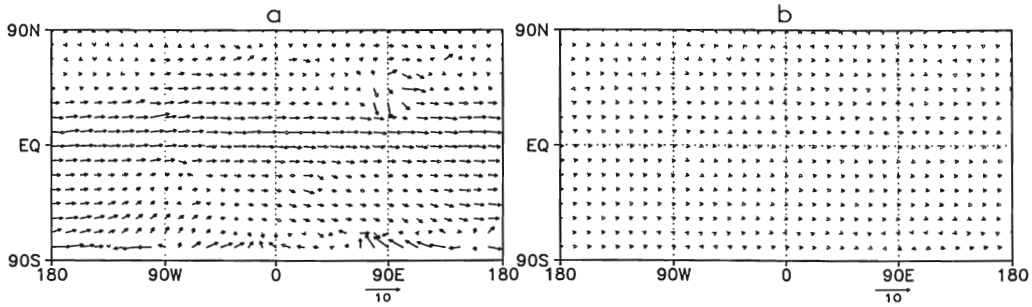

Figure 8. (a) The difference $\mathbf{v} - \mathbf{v}_b$ between the velocity field of Fig. 3a and the balanced velocity field as obtained from the corresponding potential vorticity field. (b) The difference $\mathbf{v} - \mathbf{v}_b - \mathbf{v}_a$.

parent model is around 0.5, about 20 percent of the maximum value of the latter field. For the velocity field the maximum absolute value of the difference is around 15 ms^{-1}, again about 20 percent of the maximum value of the latter field. In order to see to which extent the unbalanced velocity is important in this respect, we have repeated the integration with the unbalanced velocity $\mathbf{v}_a$ put to zero. The results are given in Figs. 9c and 9d. The maximum absolute values of the difference in potential vorticity and velocity are now around 1.5 and 35 ms^{-1}, respectively, i.e. about 50 percent of the maximum values of the parent fields. So, inclusion of the unbalanced velocity is essential for the performance of the model.

To give an idea of how the differences between parent integration and the two balanced integrations evolve in time we show in Fig. 10 as a function of time the following mean squared differences:

$$D_{P_c,P} = \frac{1}{4\pi} \int dS (P_c - P)^2, \tag{52a}$$

$$D_{\mathbf{v}_c,\mathbf{v}} = \frac{1}{4\pi} \int dS (\mathbf{v}_c - \mathbf{v})^2, \tag{52b}$$

where the unsubscripted fields refer to the parent model and the fields with a subscript c refer to the two balanced models. Using partial integration and the inner product we can write

$$D_{P_c,P} = < P_c - P, P_c - P >, \tag{53a}$$

$$D_{\mathbf{v}_c,\mathbf{v}} = - < \psi_c - \psi, \zeta_c - \zeta > - < \chi_c - \chi, \mathcal{D}_c - \mathcal{D} >, \tag{53b}$$

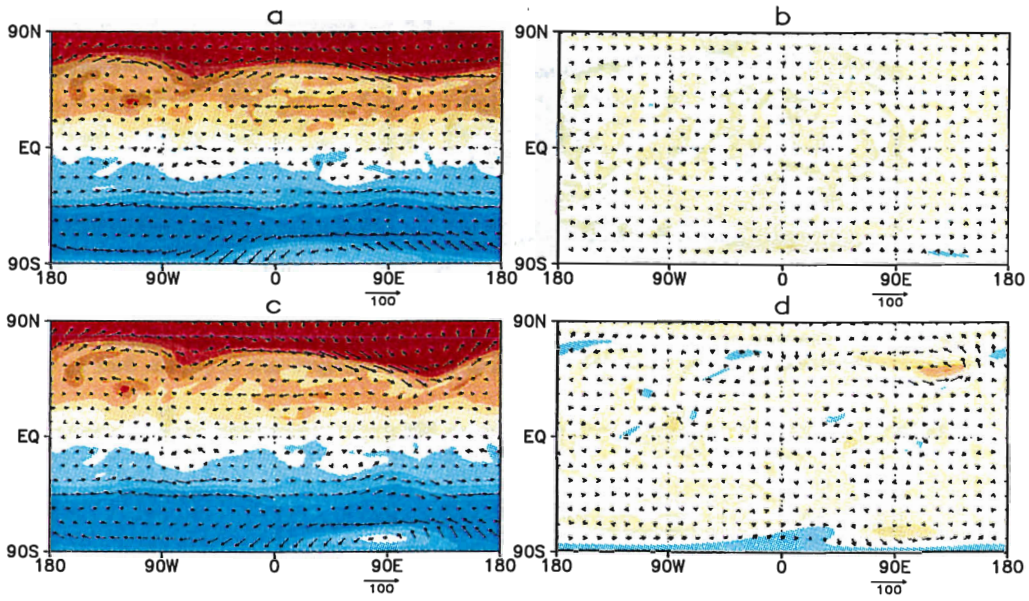

Figure 9. (a) The result at day 10 of the integration with the balanced model. The result is shown in terms of potential vorticity (colours) and velocity (arrows). In (b) the difference is shown between this end state and the end state of the parent integration, again in terms of potential vorticity (colours) and velocity (arrows). In (c) and (d) the results are shown for a balanced integration in which the unbalanced velocity is put to zero. The plotting conventions are the same as in Fig. 3

which expressions were used in the actual computations. Notice that P_c is always equal to P_b, but $\mathbf{v}_c = \mathbf{v}_b + \mathbf{v}_a$ in the full balanced integration whereas $\mathbf{v}_c = \mathbf{v}_b$ in the integration with zero unbalanced velocity. In Fig. 10a we show the value of $D_{P_c,P}$ as function of time for the two different models. The graph denoted by 'a' refers to the full balanced model; the graph denoted by 'b' refers to the balanced model with zero unbalanced velocity. We see that the diferences are very substantial, in particular at the end of the integration period. The same behaviour can be seen in a graph of $D_{\mathbf{v}_c,\mathbf{v}}$ as a function of time, shown in Fig. 10b. The graphs denoted by 'a' and 'b' refer to the same models as before and show the same kind of differences. Note that the graphs differ already at $t = 0$ because the unbalanced velocity is not included in the second case.

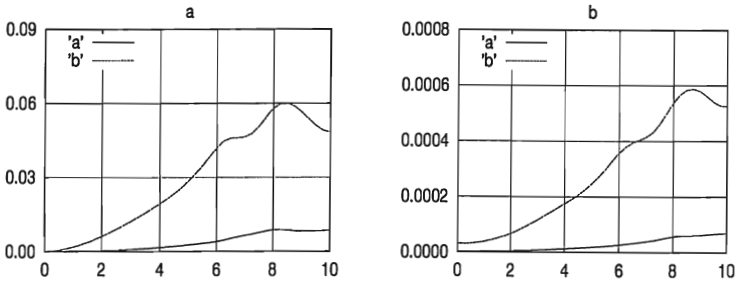

Figure 10. (a) The value of the mean squared differences $D_{P_c,P}$ and (b) $D_{\mathbf{v}_c,\mathbf{v}}$ as a function of time (in days) for the two balanced models that we consider. The graphs labelled by 'a' refers to the full balanced model; the graphs labelled by 'b' to the balanced model with zero unbalanced velocity. The graphs are based on data every 6 hours of simulated time, i.e., on 41 datapoints.

6. Summary and discussion

Salmon's method (Salmon, 1983, 1985, 1988a, 1988b, 1996) of constructing balanced approximations of geophysical fluid systems guarantees the existence of conservation laws that correspond to the conservation laws of the original (parent) systems. In the present paper Salmon's method is applied to a one-layer isentropic model of the atmosphere. Although very idealized, this is a physically consistent simplification of the atmosphere, i.e., a simplified but exact solution of the inviscid hydrostatic primitive equations. As discussed in section 2, the model is analogous to a one-layer shallow-water model and is governed by an equation for the time-change of horizontal momentum (1), an equation relating the Montgomery potential to the surface pressure (2) and an equation for the conservation of mass (4). Besides mass the model conserves potential vorticity and energy. Following Salmon, we derive in section 3 a balanced approximation of this model by formulating the momentum equation in terms of Hamilton's principle and then substituting a balanced velocity field into the Lagrangian. The balanced velocity field that is chosen, given by (18) and (19), is a simplification of 'linear balance'. This velocity field, $\mathbf{v}_b = \mathbf{k} \times \nabla f^{-1}(M - \bar{M})$, behaves acceptably on the whole sphere, in contrast with 'classic' geostrophy, $\mathbf{v}_b = \mathbf{k} \times f^{-1} \nabla M$, which forces the equator to be an impenetrable barrier between the hemispheres. Application of Hamilton's principle leads to a balanced approximation (22) of the horizontal momentum equation. Combined with the original mass conservation equation it gives a diagnostic equation (26) for the unbalanced velocity field $\mathbf{v}_a$. This equation can be transformed into two scalar equations (31). It is checked that the balanced model respects analogues of the conservation of potential vorticity and energy. Mass conservation is, by construction, incorporated in the balanced model.

The central results of this paper are (22), the balanced approximation of the momentum equation (1), and the set of equations (30)-(31) that determine the unbalanced velocity. The balanced model that we have obtained can be compared with other balanced models by considering the last term on the left-hand side of (22). If this term is zero, one obtains the 'geostrophic vorticity' approximation discussed - among many other approximations - by Allen et al. (1990a, 1990b) and Barth et al. (1990). It has many properties in common with our approximation although it has not been proved that an energy invariant exists. If 'classic' geostrophic balance had been used, the last term on the left-hand side of (22) would have been

$$\nabla[\xi_l^{-1} \mathbf{k} \cdot \nabla \times (\eta_l f^{-1} \mathbf{v}_a)]. \tag{54}$$

The difference concerns the position of the factor f^{-1}. The same holds for (25) where the factor f^{-1} would have appeared in front of the gradient operator. The resulting equation (26) would, of course, reflect these changes. We note that transforming this vector equation into scalar equations is now more involved because the first term on the left-hand side is no longer divergenceless. The most widely used alternative with which any balance approximation needs to be compared is the 'geostrophic momentum approximation' (Hoskins, 1975). In this case the last term on the left-hand side of (22) would have been, as can be easily verified from Eqs. (10) of the latter reference,

$$\mathbf{v}_a \cdot \nabla \mathbf{v}_b - \zeta_b \mathbf{k} \times \mathbf{v}_a. \tag{55}$$

In Hoskins' (1975) formulation $\mathbf{v}_b$ is given by 'classic' geostrophic balance. Also here, it is quite difficult to obtain the unbalanced velocity. To solve this problem Hoskins (1975) introduced a coordinate transformation such that fluid particles move with the geostrophic velocity. In an f-plane context this has been a very fruitful approach, allowing

solutions of many important problems. Generalizing these semi-geostrophic equations to spherical geometry, however, meets with the mentioned problem of 'classic' geostrophy, in addition to the fact that for a variable Coriolis parameter the coordinate transformation is not trivial. It is the author's opinion that, despite notable attempts to solve these problems (Shutts, 1989, Magnusdottir and Schubert, 1990, 1991, Mawson and Cullen, 1992 and Mawson, 1996), a completely satisfying solution has not been found yet. On an f-plane 'classic' geostrophic balance is identical to the approximation of linear balance that we have used. In this case the dynamics of the balanced model is the isentropic generalisation of Salmon's L_1-dynamics. The performance of Salmon's L_1-dynamics in comparison with other approximations is investigated very thoroughly for shallow-water flow on an f-plane by Allen et al. (1990a, 1990b) and Barth et al. (1990). Many references to related work can be found there.

In section 4 we discuss how the balanced model that we developed can be integrated forward in time. We take the material conservation of balanced potential vorticity as the basic prognostic equation. The surface pressure and balanced velocity can be obtained by solving a nonlinear equation relating the balanced potential vorticity to the balanced streamfunction. It is pointed out how this equation and the equation for the unbalanced velocity can be solved by iteration. To produce a benchmark against which the balanced model can be tested we discuss in section 5 a long integration with a forced and damped spectral implementation of the parent model. Within this period we select a shorter period of 10 days in which cyclogenesis occurs as a result of interaction with the model's orography. This period is rerun with the unforced and undamped parent model and taken as a reference. The result, in terms of potential vorticity and velocity fields, is shown in Fig. 3. We investigate, for the initial state, how well the underlying basic fields can be reconstructed from the potential vorticity. In this context Fig. 8 is of particular interest; this figure shows how well the velocity field is reconstructed from the potential vorticity. The figure shows that the unbalanced velocity field is important around the equator and close to high values of the orography. We then discuss a 10 day integration with the balanced model. The results are summarized in Fig. 9. The balanced integration stays close to the parent integration as can be seen from Figs. 9a and 9b. The differences at day 10 are of the order of 20 percent of the maximum values of the fields in the parent integration. Figs. 9c and 9d show that the unbalanced velocity is crucial in maintaining this degree of accuracy. This is shown in a different manner in Fig. 10.

With a time step of 2 hours the balanced model in its present state of numerical sophistication is about as fast as the parent model when in the parent model a time step of 15 minutes is used. The latter value might possibly be taken somewhat larger but not larger than 30 minutes as the model becomes numerically unstable in that case. The question arises whether the balanced model as developed here is an attractive alternative for the parent model. The answer depends on the accuracy that is required. For numerical weather prediction high accuracy is important as local weather conditions are closely tied to the details of the flow. On the other hand, for climate simulations these details matter less as long as the relevant statistics are reproduced with sufficient accuracy (Opsteegh et al., 1998). If balanced models of the type discussed in the present paper are accurate enough for a given purpose, they have an advantage over primitive equation models in that the state of the atmosphere is at any time completely given in terms of the potential vorticity field. This makes it easier to grasp the model's dynamics (Hoskins et al., 1985). Furthermore, as the basic prognostic equation is advection of balanced potential vorticity the contour-advective semi-Lagrangian (CASL) algorithm developed by Dritschel and Ambaum (1997) could be used to step such models forward in time. Because in this algorithm the potential vorticity is advected using contour advection

while the inversion of potential vorticity is carried out in an Eulerian framework, the algorithm combines advective accuracy with computational efficiency. When the balanced procedure as developed here is extended to a multilayer isentropic model, a balanced Lagrangian weather prediction model comes in sight. If the efficiency of the inversion could be improved - and this seems certainly possible - such a model could be of much use in assisting the forecaster in monitoring the numerical weather prediction process and understanding the structure and evolution of weather systems.

Acknowledgements

I would like to thank my collegues drs. U. Achatz, R.J. Haarsma, J.D. Opsteegh, F.M. Selten and R.R. Trieling of the Section Predictability Research for reading and critizing earlier versions of the manuscript. Many thanks are also due to drs. M.H.P. Ambaum and E.C. Neven and to Mr. W. Lablans whose suggestions and criticism were very helpful in giving the manuscript its present form. Finally, several anonymous referees gave constructive criticism that was useful in placing the work in a proper perspective.

Appendix A

Details on energy conservation

In this appendix we give a few details on how energy conservation can be proved in the parent model as well as in the balanced model.

(a) The parent model

To derive (12) it is convenient to use the definition of $\mathcal{H}$ as given in (17b) and repeated here for convenience:

$$\mathcal{H} = \frac{\mathbf{v}\cdot\mathbf{v}}{2} + gz_l + \frac{c_p\theta}{\kappa+1}\eta_l^{\kappa}. \tag{A.1}$$

We first note that we have

$$\frac{\partial}{\partial t}(\eta_l\mathcal{H}) = (M + \frac{\mathbf{v}\cdot\mathbf{v}}{2})\frac{\partial\eta_l}{\partial t} + \eta_l\mathbf{v}\cdot\frac{\partial\mathbf{v}}{\partial t}. \tag{A.2}$$

The partial time derivative of $\mathbf{v}$ is given by (8) and the partial time derivative of η_l by (5). Substituting these expressions gives

$$\frac{\partial}{\partial t}(\eta_l\mathcal{H}) = -(M + \frac{\mathbf{v}\cdot\mathbf{v}}{2})\nabla\cdot(\eta_l\mathbf{v}) -$$

$$\eta_l\mathbf{v}\cdot[(f+\zeta)(\mathbf{k}\times\mathbf{v}) + \nabla(M + \frac{\mathbf{v}\cdot\mathbf{v}}{2})]. \tag{A.3}$$

Using the product rule for the divergence operator to rewrite the first part in the expression at the right-hand side and deleting cancelling and zero terms, we obtain

$$\frac{\partial}{\partial t}(\eta_l\mathcal{H}) = -\nabla\cdot[(M + \frac{\mathbf{v}\cdot\mathbf{v}}{2})\eta_l\mathbf{v}], \tag{A.4}$$

which is equivalent with (12).

(b) The balanced model

To verify the conservation of balanced energy it is convenient to make use of the field $\mathcal{H}_b$ defined in (21b), which definition is repeated here:

$$\mathcal{H}_b = \frac{\mathbf{v}_b \cdot \mathbf{v}_b}{2} + gz_l + \frac{c_p\theta}{\kappa+1}\eta_l^\kappa. \tag{A.5}$$

We begin by noting that

$$\frac{\partial}{\partial t}(\eta_l\mathcal{H}_b) = (M + \frac{\mathbf{v}_b \cdot \mathbf{v}_b}{2})\frac{\partial \eta_l}{\partial t} + \eta_l\mathbf{v}_b \cdot \frac{\partial \mathbf{v}_b}{\partial t}. \tag{A.6}$$

Upon substituting (5) and (24) for the partial time derivatives of η_l and $\mathbf{v}_b$, we get

$$\frac{\partial}{\partial t}(\eta_l\mathcal{H}_b) = -(M + \frac{\mathbf{v}_b \cdot \mathbf{v}_b}{2})\nabla \cdot (\eta_l\mathbf{v}) -$$

$$\eta_l\mathbf{v}_b \cdot \{(f+\zeta_b)(\mathbf{k}\times\mathbf{v}) + \nabla[M + \frac{\mathbf{v}_b \cdot \mathbf{v}_b}{2} + (\xi_l f)^{-1})\mathbf{k} \cdot \nabla \times (\eta_l\mathbf{v}_a)]\}. \tag{A.7}$$

Using the product rule for the divergence operator to rewrite the first part in the expression on the right-hand side, writing $\mathbf{v}_b = \mathbf{v} - \mathbf{v}_a$ in the factor in front of the second term of this expression and deleting cancelling and zero terms, we obtain

$$\frac{\partial}{\partial t}(\eta_l\mathcal{H}_b) = -\nabla \cdot [(M + \frac{\mathbf{v}_b \cdot \mathbf{v}_b}{2})\eta_l\mathbf{v}] - \eta_l\mathbf{v} \cdot \nabla[(\xi_l f)^{-1}\mathbf{k} \cdot \nabla \times (\eta_l\mathbf{v}_a)] +$$

$$\eta_l\mathbf{v}_a \cdot \{(f+\zeta_b)(\mathbf{k}\times\mathbf{v}) + \nabla[M + \frac{\mathbf{v}_b \cdot \mathbf{v}_b}{2} + (\xi_l f)^{-1}\mathbf{k} \cdot \nabla \times (\eta_l\mathbf{v}_a)]\}. \tag{A.8}$$

Using the same product rule in the second term on the right-hand side of the expression above we get

$$\frac{\partial}{\partial t}(\eta_l\mathcal{H}_b) = -\nabla \cdot [(M + \frac{\mathbf{v}_b \cdot \mathbf{v}_b}{2} + (\xi_l f)^{-1}\mathbf{k} \cdot \nabla \times (\eta_l\mathbf{v}_a))\eta_l\mathbf{v}] +$$

$$[(\xi_l f)^{-1}\mathbf{k} \cdot \nabla \times (\eta_l\mathbf{v}_a)]\nabla \cdot (\eta_l\mathbf{v}) +$$

$$\eta_l\mathbf{v}_a \cdot \{(f+\zeta_b)(\mathbf{k}\times\mathbf{v}) + \nabla[M + \frac{\mathbf{v}_b \cdot \mathbf{v}_b}{2} + (\xi_l f)^{-1}\mathbf{k} \cdot \nabla \times (\eta_l\mathbf{v}_a)]\}. \tag{A.9}$$

For the second term on the right-hand side of this expression we have:

$$[(\xi_l f)^{-1}\mathbf{k} \cdot \nabla \times (\eta_l\mathbf{v}_a)]\nabla \cdot (\eta_l\mathbf{v}) =$$

$$-\nabla \cdot [(\xi_l f)^{-1}\nabla \cdot (\eta_l\mathbf{v})\ \mathbf{k} \times \eta_l\mathbf{v}_a] - \{\mathbf{k} \times \nabla[(\xi_l f)^{-1}\nabla \cdot (\eta_l\mathbf{v})]\} \cdot \eta_l\mathbf{v}_a. \tag{A.10}$$

This enables us to write

$$\frac{\partial}{\partial t}(\eta_l\mathcal{H}_b) = -\nabla \cdot [(M + \frac{\mathbf{v}_b \cdot \mathbf{v}_b}{2})\eta_l\mathbf{v}]$$

$$-\nabla \cdot [(\xi_l f)^{-1}\mathbf{k} \cdot \nabla \times (\eta_l\mathbf{v}_a)\ \eta_l\mathbf{v} + (\xi_l f)^{-1}\nabla \cdot (\eta_l\mathbf{v})\ \mathbf{k} \times \eta_l\mathbf{v}_a] +$$

$$\eta_l\mathbf{v}_a \cdot \{-\mathbf{k} \times \nabla[(\xi_l f)^{-1}\nabla \cdot (\eta_l\mathbf{v})] + (f+\zeta_b)(\mathbf{k}\times\mathbf{v}) +$$

$$\nabla[M + \frac{\mathbf{v}_b \cdot \mathbf{v}_b}{2} + (\xi_l f)^{-1}\mathbf{k} \cdot \nabla \times (\eta_l\mathbf{v}_a)]\}. \tag{A.11}$$

Now, according to (26) - which equation determines the unbalanced velocity $\mathbf{v}_a$ - the second factor in the last term of this equation is zero so that we have

$$\frac{\partial}{\partial t}(\eta_l \mathcal{H}_b) = -\nabla \cdot [(M + \frac{\mathbf{v}_b \cdot \mathbf{v}_b}{2})\eta_l \mathbf{v}]$$

$$-\nabla \cdot [(\xi_l f)^{-1}\mathbf{k} \cdot \nabla \times (\eta_l \mathbf{v}_a)\, \eta_l \mathbf{v} + (\xi_l f)^{-1}\nabla \cdot (\eta_l \mathbf{v})\, \mathbf{k} \times \eta_l \mathbf{v}_a]. \tag{A.12}$$

which equation is identical with (34).

Appendix B

Details on the variational analysis

In this appendix we will clarify some of the steps in the variational procedure. We first note that taking variations and performing partial differentiations with respect to τ, α or β are commuting operations. We will furthermore make extensive use of partial integration with respect to τ, α and β. In particular we will frequently use the following identities

$$(\frac{\partial \psi}{\partial \tau})\chi = -\psi(\frac{\partial \chi}{\partial \tau}) + \frac{\partial(\psi\chi)}{\partial \tau}, \tag{B.1a}$$

$$\frac{\partial(\psi, \chi)}{\partial(\alpha, \beta)}\xi = \psi\frac{\partial(\chi, \xi)}{\partial(\alpha, \beta)} + \frac{\partial(\psi\xi, \chi)}{\partial(\alpha, \beta)}. \tag{B.1b}$$

When integrating over τ, α and β it is assumed that all fields (including the variations) are either periodic or have zero values at the boundary of the integration domain. The second terms on the right-hand side of the expressions above therefore vanish under the integral sign.

(a) The parent model

In the following we will delete the latter contributions, so that all that follows is only valid when integrated over τ, α and β. For $\delta\mathcal{L}$ in (16) we have, for a variation $\delta\lambda$

$$\delta\mathcal{L} = \delta(ua\cos\phi\frac{\partial\lambda}{\partial\tau}) + \delta(\Omega a^2\cos^2\phi\frac{\partial\lambda}{\partial\tau}) - \delta(gz_l) - \delta(\frac{c_p\theta}{\kappa+1}\eta_l^\kappa). \tag{B.2}$$

For the first term on the right-hand side of expression (B.2) we have

$$\delta(ua\cos\phi\frac{\partial\lambda}{\partial\tau}) = ua\cos\phi\frac{\partial}{\partial\tau}\delta\lambda = -\delta\lambda\frac{\partial}{\partial\tau}(ua\cos\phi) =$$

$$-\delta\lambda\frac{Du}{Dt}a\cos\phi + \delta\lambda uv\sin\phi, \tag{B.3}$$

where in the latter equality we used that $\partial/\partial\tau = D/Dt$ and $a\partial\phi\partial\tau = u$. For the second term on the right-hand side of (B.2) we have

$$\delta(\Omega a^2\cos^2\phi\frac{\partial\lambda}{\partial\tau}) = \Omega a^2\cos^2\phi\frac{\partial}{\partial\tau}\delta\lambda = -\delta\lambda\frac{\partial}{\partial\tau}(\Omega a^2\cos^2\phi) =$$

$$\delta\lambda 2\Omega\sin\phi a^2\cos\phi\frac{\partial\phi}{\partial\tau} = \delta\lambda fva\cos\phi, \tag{B.4}$$

where we use the definition $f = 2\Omega \sin\phi$ of the Coriolis parameter and again that $a\partial\phi\partial\dot{\tau} = u$. For the third term in (B.2) we simply have

$$-\delta(gz_l) = -\delta\lambda\frac{\partial}{\partial\lambda}(gz_l). \tag{B.5}$$

The calculation of the last term in (B.2) is somewhat more involved. First of all we note that

$$-\delta(\frac{c_p\theta}{\kappa+1}\eta_l^\kappa) = -\frac{\kappa c_p\theta}{\kappa+1}\eta_l^{\kappa-1}\delta\eta_l. \tag{B.6}$$

Now, according to expression (14) of section 2 we may write

$$\delta\eta_l = -\eta_l^2\delta\eta_l^{-1} = -\eta_l^2(\frac{p_r}{g})a^2\cos\phi\frac{\partial(\delta\lambda,\phi)}{\partial(\alpha,\beta)}, \tag{B.7}$$

so that

$$-\delta(\frac{c_p\theta}{\kappa+1}\eta_l^\kappa) = \frac{\kappa c_p\theta}{\kappa+1}\eta_l^{\kappa+1}(\frac{p_r}{g})a^2\cos\phi\frac{\partial(\delta\lambda,\phi)}{\partial(\alpha,\beta)} =$$

$$\delta\lambda\frac{\partial(\phi,\frac{\kappa c_p\theta}{\kappa+1}\eta_l^{\kappa+1}(\frac{p_r}{g})a^2\cos\phi)}{\partial(\alpha,\beta)} =$$

$$\delta\lambda\frac{\partial(\phi,\frac{\kappa c_p\theta}{\kappa+1}\eta_l^{\kappa+1}(\frac{p_r}{g})a^2\cos\phi)}{\partial(\lambda,\phi)}\frac{\partial(\lambda,\phi)}{\partial(\alpha,\beta)}. \tag{B.8}$$

Therefore, using the definition of the Jacobian and expression (14) we can write

$$-\delta(\frac{c_p\theta}{\kappa+1}\eta_l^\kappa) = -\delta\lambda\eta_l^{-1}\frac{\partial}{\partial\lambda}(\frac{\kappa c_p\theta}{\kappa+1}\eta_l^{\kappa+1}) = -\delta\lambda\frac{\partial}{\partial\lambda}(c_p\theta\eta_l^\kappa). \tag{B.9}$$

So we have

$$-\delta(gz_l) - \delta(\frac{c_p\theta}{\kappa+1}\eta_l^\kappa) = -\delta\lambda\frac{\partial M}{\partial\lambda}. \tag{B.10}$$

This gives us for $\delta\mathcal{L}$:

$$\delta\mathcal{L} = -a\cos\phi\delta\lambda(\frac{Du}{Dt} - uv\frac{\tan\phi}{a} - fv + \frac{1}{a\cos\phi}\frac{\partial M}{\partial\lambda}). \tag{B.11}$$

Integrating this over τ, α and β leads to the zonal component of (1). In a similar way we may derive the meridional component of (1) by considering variations $\delta\phi$. This derivation is somewhat more complicated because some of the metric terms need to be differentiated with respect to ϕ. In the end these extra contributions cancel out.

(b) The balanced model

The starting point here is

$$\delta\mathcal{L}_b = \delta(u_b a\cos\phi\frac{\partial\lambda}{\partial\tau}) + \delta(\Omega a^2\cos^2\phi\frac{\partial\lambda}{\partial\tau}) + \delta(v_b a\frac{\partial\phi}{\partial\tau}) -$$

$$\delta(\frac{u_b^2+v_b^2}{2}) - \delta(gz_l) - \delta(\frac{c_p\theta}{\kappa+1}\eta_l^\kappa). \tag{B.12}$$

From the foregoing it is clear that we have

$$\delta(u_b a\cos\phi\frac{\partial\lambda}{\partial\tau}) = u\delta u_b - \delta\lambda\frac{Du_b}{Dt}a\cos\phi + \delta\lambda u_b v\sin\phi, \tag{B.13a}$$

$$\delta(\Omega a^2\cos^2\frac{\partial\lambda}{\partial\tau}) = \delta\lambda f v a\cos\phi, \tag{B.13b}$$

$$\delta(v_b a\frac{\partial\phi}{\partial\tau}) = v\delta v_b, \tag{B.13c}$$

$$-\delta(\frac{u_b^2+v_b^2}{2}) = -u_b\delta u_b - v_b\delta v_b, \tag{B.13d}$$

$$-\delta(gz_l) - \delta(\frac{c_p\theta}{\kappa+1}\eta_l^\kappa) = -\delta\lambda\frac{\partial M}{\partial\lambda}, \tag{B.13e}$$

so that

$$\delta\mathcal{L}_b = u_a\delta u_b + v_a\delta v_b -$$
$$a\cos\phi\delta\lambda(\frac{Du_b}{Dt} - u_b v\frac{\tan\phi}{a} - fv + \frac{1}{a\cos\phi}\frac{\partial M}{\partial\lambda}), \tag{B.14}$$

where $u_a = u - u_b$ and $v_a = v - v_b$ are the zonal and meridional components of the unbalanced velocity. We have, using (14) and (18),

$$u_a\delta u_b = u_a\delta(-\frac{1}{a}\frac{\partial\psi_b}{\partial\phi}) = \frac{u_a}{a}\delta[\frac{\partial(\psi_b,\lambda)}{\partial(\lambda,\phi)}] = u_a a\cos\phi(\frac{p_r}{g})\delta[\frac{\partial(\psi_b,\lambda)}{\partial(\alpha,\beta)}\eta_l]. \tag{B.15}$$

This gives

$$u_a\delta u_b = u_a a\cos\phi(\frac{p_r}{g})\frac{\partial(\delta\psi_b,\lambda)}{\partial(\alpha,\beta)}\eta_l +$$
$$u_a a\cos\phi(\frac{p_r}{g})\frac{\partial(\psi_b,\delta\lambda)}{\partial(\alpha,\beta)}\eta_l + u_a a\cos\phi(\frac{p_r}{g})\frac{\partial(\psi_b,\lambda)}{\partial(\alpha,\beta)}\delta\eta_l. \tag{B.16}$$

For the second and third term in the expression for $u_a\delta u_b$ we can derive, using (B.1), (B.7), (14) and the expression for the balanced velocity (18),

$$u_a a\cos\phi(\frac{p_r}{g})\frac{\partial(\psi_b,\delta\lambda)}{\partial(\alpha,\beta)}\eta_l = \delta\lambda[-\eta_l^{-1}v_b\frac{\partial}{\partial\phi}(\cos\phi\eta_l u_a) - \eta_l^{-1}u_b\frac{\partial}{\partial\lambda}(\eta_l u_a)], \tag{B.17}$$

$$u_a a\cos\phi(\frac{p_r}{g})\frac{\partial(\psi_b,\lambda)}{\partial(\alpha,\beta)}\delta\eta_l = \delta\lambda[\eta_l^{-1}u_b\frac{\partial}{\partial\lambda}(\eta_l u_a) + u_a\frac{\partial u_b}{\partial\lambda}]. \tag{B.18}$$

The calculation of the first term in the expression of $u_a\delta u_b$ is somewhat more involved. We first derive, using (B.1) and (14),

$$u_a a\cos\phi(\frac{p_r}{g})\frac{\partial(\delta\psi_b,\lambda)}{\partial(\alpha,\beta)}\eta_l = \delta\psi_b\eta_l^{-1}\frac{1}{a\cos\phi}\frac{\partial}{\partial\phi}(\cos\phi\eta_l u_a). \tag{B.19}$$

Then we note that, by the balance condition (19) and (B.7),

$$\delta\psi_b = \frac{1}{f}\delta M = \frac{1}{f}\delta(gz_l + c_p\theta\eta_l^\kappa) =$$

$$\frac{1}{f}\frac{\partial}{\partial\lambda}(gz_l)\delta\lambda - \frac{1}{f}\kappa c_p\theta\eta_l^{\kappa+1}\frac{p_r}{g}a^2\cos\phi\frac{\partial(\delta\lambda,\phi)}{\partial(\alpha,\beta)}. \tag{B.20}$$

Substituting (B.20) into (B.19) and applying (B.1) and (14) we obtain

$$u_a a\cos\phi(\frac{p_r}{g})\frac{\partial(\delta\psi_b,\lambda)}{\partial(\alpha,\beta)}\eta_l = \delta\lambda\frac{1}{f}\frac{\partial}{\partial\lambda}(gz_l)\eta_l^{-1}\frac{1}{a\cos\phi}\frac{\partial}{\partial\phi}(\cos\phi\eta_l u_a)+$$

$$\delta\lambda\frac{1}{f}\frac{\partial}{\partial\lambda}[\kappa c_p\theta\eta_l^{\kappa}\frac{1}{a\cos\phi}\frac{\partial}{\partial\phi}(\cos\phi\eta_l u_a)]\eta_l^{-1}. \tag{B.21}$$

Now, applying the product rule of differentiation on the second term of the right-hand side of (B.21) and using the expression (2) of the Montgomery potential we derive

$$u_a a\cos\phi(\frac{p_r}{g})\frac{\partial(\delta\psi_b,\lambda)}{\partial(\alpha,\beta)}\eta_l = \delta\lambda\frac{1}{f}\frac{\partial M}{\partial\lambda}\eta_l^{-1}\frac{1}{a\cos\phi}\frac{\partial}{\partial\phi}(\cos\phi\eta_l u_a)+$$

$$\delta\lambda\frac{1}{f}\eta_l^{-1}\frac{\partial}{\partial\lambda}[(\kappa-1)c_p\theta\eta_l^{\kappa}]\frac{1}{a\cos\phi}\frac{\partial}{\partial\phi}(\cos\phi\eta_l u_a)+$$

$$\delta\lambda\frac{1}{f}[\kappa c_p\theta\eta_l^{\kappa-1}]\frac{\partial}{\partial\lambda}(\frac{1}{a\cos\phi}\frac{\partial}{\partial\phi}(\cos\phi\eta_l u_a)). \tag{B.22}$$

Using expressions (18) and (19) for the balanced velocity, we may write

$$\frac{1}{f}\frac{\partial M}{\partial\lambda} = a\cos\phi v_b. \tag{B.23}$$

We furthermore have

$$\eta_l^{-1}\frac{\partial}{\partial\lambda}[(\kappa-1)c_p\theta\eta_l^{\kappa}] = \frac{\partial}{\partial\lambda}[\kappa c_p\theta\eta_l^{\kappa-1}]. \tag{B.24}$$

This enables us to write

$$u_a a\cos\phi(\frac{p_r}{g})\frac{\partial(\delta\psi_b,\lambda)}{\partial(\alpha,\beta)}\eta_l =$$

$$\delta\lambda[\eta_l^{-1}v_b\frac{\partial}{\partial\phi}(\cos\phi\eta_l u_a) + \frac{\partial}{\partial\lambda}(\frac{1}{f}\kappa c_p\theta\eta_l^{\kappa-1}\frac{1}{a\cos\phi}\frac{\partial}{\partial\phi}(\cos\phi\eta_l u_a))]. \tag{B.25}$$

Combining (B.16), (B.17), (B.18) and (B.25) we thus obtain

$$u_a\delta u_b = \delta\lambda[u_a\frac{\partial u_b}{\partial\lambda} + \frac{\partial}{\partial\lambda}(\frac{1}{f}\kappa c_p\theta\eta_l^{\kappa-1}\frac{1}{a\cos\phi}\frac{\partial}{\partial\phi}(\cos\phi\eta_l u_a))]. \tag{B.26}$$

In a similar way we may derive that

$$v_a\delta v_b = \delta\lambda[v_a\frac{\partial v_b}{\partial\lambda} - \frac{\partial}{\partial\lambda}(\frac{1}{f}\kappa c_p\theta\eta_l^{\kappa-1}\frac{1}{a\cos\phi}\frac{\partial}{\partial\lambda}(\eta_l v_a))], \tag{B.27}$$

so that

$$u_a\delta u_b + v_a\delta v_b = -a\cos\phi\delta\lambda[-\frac{u_a}{a\cos\phi}\frac{\partial u_b}{\partial\lambda} - \frac{v_a}{a\cos\phi}\frac{\partial v_b}{\partial\lambda}+$$

$$\frac{1}{a\cos\phi}\frac{\partial}{\partial\lambda}(\frac{1}{f}\kappa c_p\theta\eta_l^{\kappa-1}\mathbf{k}\cdot\nabla\times(\eta_l\mathbf{v}_a))]. \tag{B.28}$$

(For a concise list of horizontal vector operators in spherical coordinates we refer to Verkley (2000).) Combining this expression with (B.14) we obtain

$$\delta\mathcal{L}_b = -a\cos\phi\delta\lambda[-\frac{u_a}{a\cos\phi}\frac{\partial u_b}{\partial\lambda} - \frac{v_a}{a\cos\phi}\frac{\partial v_b}{\partial\lambda} + \frac{Du_b}{Dt} - u_b v\frac{\tan\phi}{a}$$

$$-fv + \frac{1}{a\cos\phi}\frac{\partial M}{\partial\lambda} + \frac{1}{a\cos\phi}\frac{\partial}{\partial\lambda}(\frac{1}{f}\kappa c_p\theta\eta_l^{\kappa-1}\mathbf{k}\cdot\nabla\times(\eta_l\mathbf{v}_a))]. \tag{B.29}$$

Using that, (see (B.3),

$$-\frac{v_a}{a\cos\phi}\frac{\partial v_b}{\partial\lambda} = -v_a[\zeta_b + \frac{1}{a\cos\phi}\frac{\partial(\cos\phi u_b)}{\partial\phi}] = -v_a\zeta_b + u_b v_a\frac{\tan\phi}{a} - \frac{v_a}{a}\frac{\partial u_b}{\partial\phi}, \tag{B.30}$$

we can write

$$\delta\mathcal{L}_b = -a\cos\phi\delta\lambda[-\frac{u_a}{a\cos\phi}\frac{\partial u_b}{\partial\lambda} - \frac{v_a}{a}\frac{\partial u_b}{\partial\phi} + \frac{Du_b}{Dt} - u_b v_b\frac{\tan\phi}{a}$$

$$-fv_b + \frac{1}{a\cos\phi}\frac{\partial M}{\partial\lambda} - (f+\zeta_b)v_a + \frac{1}{a\cos\phi}\frac{\partial}{\partial\lambda}(\frac{1}{f}\kappa c_p\theta\eta_l^{\kappa-1}\mathbf{k}\cdot\nabla\times(\eta_l\mathbf{v}_a))]. \tag{B.31}$$

Finally, substituting the field ξ introduced in (23) to simplify the last term in (B.31) and using that

$$-\frac{u_a}{a\cos\phi}\frac{\partial u_b}{\partial\lambda} - \frac{v_a}{a}\frac{\partial u_b}{\partial\phi} + \frac{Du_b}{Dt} = \frac{D_b u_b}{Dt}, \tag{B.32}$$

we have

$$\delta\mathcal{L}_b = -a\cos\phi\delta\lambda[\frac{D_b u_b}{Dt} - u_b v_b\frac{\tan\phi}{a} - fv_b + \frac{1}{a\cos\phi}\frac{\partial M}{\partial\lambda} -$$

$$(f+\zeta_b)v_a + \frac{1}{a\cos\phi}\frac{\partial}{\partial\lambda}((\xi_l f)^{-1}\mathbf{k}\cdot\nabla\times(\eta_l\mathbf{v}_a))]. \tag{B.33}$$

Integrating this expression over τ, α and β leads to the zonal component of the balanced approximation (22) of the momentum equation. In a similar way - albeit with a few complications due to differentiations of the metric coefficients with respect to ϕ - we may derive the meridional component of (22).

References

Allen, J.S., J.A. Barth, and P.A. Newberger	1990a	On intermediate models for barotropic continental shelf and slope flow fields. Part I: Formulation and comparison of exact solutions. *J. Phys. Oceanogr.*, **20**, 1017-1042
Allen, J.S., J.A. Barth, and P.A. Newberger	1990b	On intermediate models for barotropic continental shelf and slope flow fields. Part III: Comparision of numerical model solutions in periodic channels. *J. Phys. Oceanogr.*, **20**, 1949-1973
Barth, J.A., J.S. Allen, and P.A. Newberger	1990	On intermediate models for barotropic continental shelf and slope flow fields. Part II: Comparision of numerical model solutions in doubly periodic channels.*J. Phys. Oceanogr.*, **20**, 1044-1076
Daley, R.	1983	Linear non-divergent mass-wind laws on the sphere. *Tellus*, **35A**, 17-27
Dritschel, D.G. and M.H.P. Ambaum	1997	A contour-advective semi-Lagrangian numerical algorithm for simulating fine-scale conservative dynamical fields. *Q.J.R. Meteorol. Soc.*, **123**, 1097-1130

Dutton, J.A.	1986	*The Ceaseless Wind, An Introduction to the Theory of Atmospheric Motion*, Dover
Hoskins, B.J.	1975	The geostrophic momentum approximation and the semi-geostrophic equations. *J. Atmos. Sci.*, **32**, 233-243
Hoskins, B.J., M.E. McIntyre, and A.W. Robertson	1985	On the use and significance of isentropic potential-vorticity maps. *Q.J.R. Meteorol. Soc.*, **111**, 877-946
Lynch, P	1989	The slow equations. *Q.J.R. Meteorol. Soc.* **115**, 201-219
Machenhauer, B.	1979	The spectral method. *Numerical Methods Used in Atmospheric Models, Vol II.* WMO/GARP Publ. Ser. 17, 121-275
Magnusdottir, G. and W.H. Schubert	1990	The generalisation of semigeostrophic theory to the β-plane. *J. Atmos. Sci.* **47**, 1714-1720
Magnusdottir, G. and W.H. Schubert	1991	Semigeostrophic theory on the hemisphere. *J. Atmos. Sci.* **48**, 1449-1456
Mawson, M.H.	1996	A shallow-water semi-geostrophic model on a sphere. *Q.J.R. Meteorol. Soc.* **122**, 267-290
Mawson, M.H. and M.J.P. Cullen	1992	An idealized simulation of the Indian monsoon using primitive-equation and quasi-equilibrium models. *Q.J.R. Meteorol. Soc.* **118**, 153-164
Opsteegh, J.D., R.J. Haarsma, F.M. Selten, and A. Kattenberg	1998	ECBILT: a dynamic alternative to mixed boundary conditions in ocean models. *Tellus*, **50A**, 348-367
Salmon, R.	1983	Practical use of Hamilton's principle. *J. Fluid Mech.* **132**, 431-444
Salmon, R.	1985	New equations for nearly geostrophic flow. *J. Fluid Mech.* **153**, 461-477
Salmon, R.	1988a	Hamiltonian fluid mechanics. *Ann. Rev. Fluid Mech.* **20**, 225-256
Salmon, R.	1988b	Semigeostrophic theory as a Dirac-bracket projection. *J. Fluid Mech.* **196**, 345-358
Salmon, R.	1996	Large-scale semigeostrophic equations for use in ocean circulation modelds. *J. Fluid Mech.* **318**, 85-105
Shutts, G.J.	1989	Planetary semi-geostrophic equations derived from Hamilton's principle. *J. Fluid Mech.* **208**, 545-573
Verkley, W.T.M.	2000	On the vertical velocity in an isentropic layer. *Q.J.R. Meteorol. Soc.* **126**, 263-274

KNMI-PUBLICATIES, VERSCHENEN SEDERT 1998

Een overzicht van eerder verschenen publicaties, wordt verzoek toegezonden door de Bibliotheek van het KNMI, postbus 201, 3730 AE De Bilt, tel. 030 - 2 206 855, fax. 030 - 2 210 407; e-mail: biblioth@knmi.nl

▼ KNMI-PUBLICATIE MET NUMMER

150-28 Sneeuwdek in Nederland 1961-1990 / A.M.G. Klein Tank
181b FM12 SYNOP · internationale en nationale regelgeving voor het coderen van de groepen 7wwW1W2 en 960ww; derde druk
183-1 Rainfall in New Guinea (Irian Jaya) / T.B. Ridder
183-2 Vergelijking van zware regens te Hollandia (Nieuw Guinea), thans Jayapura (Irian Jaya) met zware regens te De Bilt / T. B. Ridder
183-3 Verdamping in Nieuw-Guinea, vergelijking van gemeten hoeveelheden met berekende hoeveelheden / T.B. Ridder
183-4 Beschrijving van het klimaat te Merauke, Nieuw Guinea, in verband met de eventuele vestiging van een zoutwinningsbedrijf / T.B. Ridder a.o.
183-5 Overzicht van klimatologische en geofysische publikaties betreffende Nieuw-Guinea / T.B. Ridder
184a Inleiding tot de algemene meteorologie : studie-uitgave ; 2e druk / B. Zwart, A. Steenhuisen, m.m.v. H.J. Krijnen
185a Handleiding voor het gebruik van sectie 2 van de FM 13-X SHIP-code voor waarnemers op zee / KNMI; KLu; KM
186-I Rainfall generator for the Rhine Basin: single-site generation of weather variables by nearest-neighbour resampling / T. Brandsma a.o.
186-II Rainfall generator for the Rhine Basin: multi-site generation of weather variables by nearest-neighbour resampling / T. Brandsma a.o.
186-III Rainfall generator for the Rhine Basin: nearest-neighbour resampling of daily circulation indices and conditional generation of weather variables / Jules J. Beersma and T. Adri Buishand
187 De wind in de rug: KNMI-weerman schaatst de Elfstedentocht / H. van Dorp
188 SODA workshop on chemical data assimilation: proceedings; 9-10 December 1998, KNMI, De Bilt, The Netherlands
189 Aardbevingen in Noord-Nederland in 1998: met overzichten over de periode 1986-1998 / [Afdeling Seismologie]
190 Seismisch netwerk Noord-Nederland / [afdeling Seismologie]

▼ TECHNISCH RAPPORT = TECHNICAL REPORT (TR)

176 Verification of the WAQUA/CSM-16 model for the winters 1992-93 and 1993-94 / J.W. de Vries
177 Nauwkeuriger nettostraling meten / M.K. van der Molen en W. Kohsiek
178 Neerslag in het stroomgebied van de Maas in januari 1995: waarnemingen en verificatie van modelprognoses / R.Jilderda a.o.
179 First field experience with 600PA phased array sodar / H. Klein Baltink
180 Een Kalman-correctieschema voor de wegdektemperatuurverwachtingen van het VAISALA-model / A. Jacobs
181 Calibration study of the K-Gill propeller vane / Marcel Bottema
182 Ontwikkeling van een spectraal UV-meetinstrument / Frank Helderman
183 Rainfall generator for the Rhine catchment : a feasibility study / T. Adri Buishand and Theo Brandsma
184 Parametrisatie van mooi-weer cumulus / M.C. van Zanten
185 Interim report on the KNMI contributions to the second phase of the AERO-project / Wiel Wauben, Paul Fortuin a.o.
186 Seismische analyse van de aardbevingen bij Middelstum (30 juli 1994) en Annen (16 augustus '94 en 31 januari '95) / [Seismologisch Onderzoek]
187 Analyse wenselijkheid overname RIVM-windmeetlokaties door KNMI / H. Benschop
188 Windsnelheidsmetingen op zeestations en kuststations: herleiding waarden windsnelheden naar 10-meter niveau / H. Benschop
189 On the KNMI calibration of net radiometers / W. Kohsiek
190 NEDWAM statistics over the period October 1994 - April 1995 / F.B. Koek
191 Description and verification of the HIRLAM trajectory model / E. de Bruijn
192 Tiltmeting · een alternatief voor waterpassing ? / H.W. Haak
193 Error modelling of scatterometer, in-situ and ECMWF model winds; a calibration refinement / Ad Stoffelen
194 KNMI contribution to the European project POPSICLE / Theo Brandsma a.o.
195 ECBILT · a coupled atmosphere ocean sea-ice model for climate predictability studies / R.J. Haarsma a.o.
196 Environmental and climatic consequences of aviation: final report of the KNMI contributions to the AERO-project / W. Wauben a.o.
197 Global radiation measurements in the operational KNMI meteorological network: effects of pollution and ventilation / F. Kuik
198 KALCORR: a kalman-correction model for real-time road surface temperature forecasting / A. Jacobs
199 Macroseismische waarnemingen Roswinkel 19-2-1997 / B. Dost e.a.
200 Operationele UV-metingen bij het KNMI / F. Kuik
201 Vergelijking van de Vaisala's HMP233 en HMP243 relatieve luchtvochtigheidsmeters / F Kuik
202 Statistical guidance for the North Sea / Janet Wijngaard and Kees Kok
203 UV-intercomparison SUSPEN / Foeke Kuik and Wiel Wauben
204 Temperature corrections on radiation measurements using Modtran 3 / D.A. Bunskoek, A.C.A.P. van Lammeren and A.J. Feijt
205 Seismisch risico in Noord-Nederland / Th. De Crook, H.W. Haak en B. Dost
206 The HIRLAM-STAT-archive and its application programs / Albert Jacobs
207 Retrieval of aerosol properties from multispectral direct sun measurements / O.P. Hasekamp
208 The KNMI Garderen Experiment, micro-meteorological observations 1988-1989; instruments and data / F.C. Bosveld a.o.
209 CO2 in water and air during ASGAMAGE: concentration measurements and consensus data / Cor M.J. Jacobs, Gerard J. Kunz, Detlev Sprung a.o.
210 Elf jaar Cabauw-metingen / J.G. van der Vliet
211 Indices die de variabiliteit en de extremen van het klimaat beschrijven / E.J Klok
212 First guess TAF-FGTAF: semi-automation in TAF production / Albert Jacobs
213 Zeer korte termijn bewolkingsverwachting met behulp van METCAST: een verificatie en beschrijving model-uitvoer / S.H. van der Veen
214 The implementation of two mixed-layer schemes in the HOPE ocean general circulation model / M. van Eijk
215 Stratosphere-troposphere exchange of ozone, diagnosed from an ECMWF ozone simulation experiment / Harm Luykx
216 Evaluatierapport Automatisering Visuele Waarnemingen Ontwikkeling Meestsystemen / Wiel Wauben en Hans de Jongh
217 Verificatie TAF en TREND / Hans van Bruggen
218 LEO - LSG and ECBILT coupled through OASIS: description and manual/A. Sterl
219 De invloed van de grondwaterstand, wind, temperatuur en dauwpunt op de vorming van stralingsmist: een kwantitatieve benadering / Jan Terpstra
220 Back-up modellering van windmeetmasten op luchthavens / Ilja Smits
221 PV-mixing around the tropopause in an extratropical cyclone / M. Sigmond
222 NPK-TIG oefendag 16 december 1998 / G.T. Geertsema, H. van Dorp e.a.
223 Golfhoogteverwachtingen voor de Zuidelijke Noordzee: een korte vergelijking van het ECMWF-golfmodel (EPS en operationeel), de nautische gidsverwachting, Nedwam en meteoroloog / D.H.P Vogelezang en C.J. Kok.
224 HDFg library and some HDF utilities: an extention to the NCSA HDF library user's manual & reference guide / Han The
225 The Deelen Infrasound Array: on the detection and identification of infrasound / L.G. Evers and H.W. Haak
226 2D Variational Ambiguity Removal / J.C.W. de Vries and A.C.M. Stoffelen

▼ WETENSCHAPPELIJK RAPPORT = SCIENTIFIC REPORT (WR)

97-01 The adjoint of the WAM model / H. Hersbach
97-02 Optimal interpolation of partitions: a data assimilation scheme for NEDWAM-4; description and evaluation of the period November 1995 - October 1996 / A.Voorrips
97-03 SATVIEW: a semi-physical scatterometer algorithm / J.A.M. Janssen a.o.
97-04 GPS water vapour meteorology status report / H. Derks a.o.
97-05 Climatological spinup of the ECBILT oceanmodel / Arie Kattenberg a.o
97-06 Direct determination of the air-sea transfer velocity of CO2 during ASGAMAGE / J.C.M. Jacobs, W. Kohsiek and W.A. Oost
97-07 Scattering matrices of ice crystals / M. Hess, P. Stammes a.o.
97-08 Experiments with horizontal diffusion and advection in a nested fine mesh mesoscale model / E.I.F. de Bruijn
97-09 On the assimilation of ozone into an atmospheric model / E.Valur Hólm
98-01 Steady state analysis of a coupled atmosphere ocean-boxmodel / F.A. Bakker
98-02 The ASGAMAGE workshop, September 22-25, 1997 / ed. W.A. Oost
98-03 Experimenting with a similarity measure for atmospheric flows / R.A. Pasmanter and X.-L. Wang
98-04 Evaluation of a radio interferometry lightning positioning system / H.R.A. Wessels
98-05 Literature study of climate effects of contrails caused by aircraft emissions / V.E. Pultau
99-01 Enhancement of solar and ultraviolet surface irradiance under partial cloudy conditions / Serdal Tunç
99-02 Turbulent air flow over sea waves: simplified model for applications / V.N. Kudryavtsev, V.K. Makin and J.F. Meirink
99-03 The KNMI Garderen experiment, micro-meteorological observations 1988-1989: corrections / Fred C. Bosveld
99-04 ASGAMAGE: the ASGASEX MAGE experiment final report / ed. W.A.Oost
2000-01 A model of wind transformation over water-land surfaces / V.N Kudryavtsev, V.K. Makin, A.M.G. Klein Tank and J.W Verkaik
2000-02 On the ait-sea coupling in the WAM wave model / D.F.Doortmont and V K. Makin.
2000-03 Salmon's Hamiltonian approach to balanced flow applied to a on-elayer isentropic model of the atmosphere / W.T.M. Verkley